UiT
THE ARCTIC
UNIVERSITY
OF NORWAY

FACULTY OF SCIENCE AND TECHNOLOGY
Department of Physics and Technology

Iceberg Drift-Trajectory Modelling and Probability Distribution of the Predictions

Ole Baadshaug

EOM-3901: Master Thesis in Energy, Climate and Environment 30SP, June 2018

“I enjoy chaos and disorder ... you see, I’m an entropy fan.”
–George Carlin

Abstract

Moving icebergs represent a major problem for shipping, as well as for oil and gas installations in ice infested waters. To be able to take actions against hazardous icebergs, it is necessary to develop models for prediction of iceberg drift trajectories. Many models have been developed in order to do so, using different approaches. These approaches can be divided into two main categories, *dynamic* models and *statistical* models. The main difference between the approaches is that dynamic models forecast drift relying on the Newtonian equations utilizing forcing data, while the statistical models are based on an optimum statistical prediction using prior velocities to forecast the drift. This thesis will present the general physical and statistical theory iceberg drift models rely upon, and review a selection of different iceberg models.

The main goal of this thesis is to evaluate the forecasting capabilities of two different iceberg drift models, implemented in a software module called *OpenBerg*. A model making accurate drift predictions could be utilized both operationally, and for research purposes. One of the models is a deterministic model, relying on dynamic equations. The other is a hybrid model which utilizes dynamic forecasting of components considered predictable (such as winds and tides), while modelling the residual component using statistical methods.

To evaluate the software module, sensitivity studies were utilized to determine the effect of certain parameter choices. An ensemble analysis was performed on a selected track section, and the results were used to create confidence bounds for the predictions.

Acknowledgements

First of all, I would like to thank my supervisors Torbjørn Eltoft and Rune Graversen for the helpful discussions and valuable feedback on this thesis. I am particularly thankful for the proof-reading, and the help finding the necessary data sets.

I am grateful to my co-supervisors Ron Saper and Knut-Frode Dagestad for providing the model software. A special thanks to you both for helping me solve the problems that popped up, all the way to the finish line.

Many thanks to Thomas Kræmer for being helpful and patient when I was blind to the nuances of the Python language. Thank you Martine Espeseth, Johannes Lohse and Cornelius Quigley for many helpful discussions.

To fellow my students, EKM class of '13, thank you for five awesome years! A special shout-out to the other master students at CIRFA, for the long hours at the ping-pong table.

To my whole family: Thank you for your continuous nagging, teasing, love and occasional support! Without you none of this would have been possible. Thank you Jostein, for taking the time to proof-read.

Finally, to my girlfriend Anna. Thank you for proof-reading my thesis and making life worth living!

Contents

List of Figures

List of Tables

List of Abbreviations

2D two dimensional

ACF autocorrelation function

CDI Climate Data Interface

CDO Climate Data Operators

CIS Canadian Ice Service

ERA-Interim European Reanalysis-Interim

ERA5 European Reanalysis 5

GODAE the Global Ocean Data Assimilation Experiment

GPS Global Positioning System

GUI graphical user interface

MSE mean square error

NCO netCDF Operators

RIOPS Regional Ice Ocean Prediction System

RMSE root mean square error

SD standard deviation

UO the University of Ottawa

1 Introduction

Drifting icebergs can represent major problems for shipping traffic, as well as for oil and gas installations. The icebergs represent hazards to the lives and health of people working in the danger zones, as well as to property such as ships and oil platforms. Ever since the RMS "Titanic" famously sank after colliding with an iceberg in the North Atlantic Ocean in April of 1912, intensive efforts have been made to chart iceberg positions (Bigg et al., 1996). Nevertheless, icebergs continues to this day to be dangerous for various operations in ice infested regions. Due to the danger they represent, it is important to monitor and predict the drift trajectory of icebergs, in order to be able to take actions against those that are hazardous.

1.1 Background

Many models have been developed in order to predict iceberg drift trajectories. The most intuitive approach to modelling iceberg drift is by using a Newtonian dynamic approach. In such models all significant forcing components are required to be specified separately in terms of physical parameters associated with the iceberg itself and the surrounding environments (Marko et al., 1988). Experiences with such models have shown that they are sensitive to errors in the forecasts of various forcing components. Especially the sea water velocity has proven difficult to predict (Garrett, 1985). As this is a major forcing component, it makes dynamic iceberg drift prediction very sensitive to errors in the input

data representing the forcing fields due to currents.

Due to these limitations of dynamic approaches, statistical approaches to iceberg drift modelling have been developed. These models allows the dynamics of the iceberg motion to be excluded from the computations. The input information is instead derived from recent observed iceberg motions. This approach produce predictions in the form of relative probabilities of possible trajectories based on the previous observations. The correlation between the observed motion and predicted motion is diminishing the further into the future we predict. When making forecasts on a long term basis, the predicted positions will eventually be completely based on estimated values. Thus, small errors in the short term prediction becomes large in the long term. Therefore the statistical models are only considered applicable to short term forecasting.

1.2 Scope

This thesis will look into iceberg drift modelling from a few angles. First a survey of existing iceberg drift models is presented. Some space is also used to describe the theoretical dynamics and statistics these models are commonly based upon. It will in closer detail examine one particular deterministic model and one statistical model in order to give a deeper understanding of different approaches to the forecasting of iceberg drift trajectories.

In addition, a recently developed software module has been made available for testing. This module is designed for comparing the performance of two different iceberg trajectory models. One is a model based on the statistical approach, but is designed to also include certain dynamic components. The other is a dynamic model, using a deterministic approach to create the drift forecast. The module, named *OpenBerg*, was developed by Ron Saper at the Water and Ice Research Laboratory, Carleton University Department of Geography and Environmental Studies. It is operating within the *OpenDrift* framework, which was developed by Knut-Frode Dagestad at the Norwegian Meteorological Institute.

The review will include test runs of OpenBerg compared to observational data to evaluate the performance. This data includes observed iceberg trajectories from the Baffin Bay, off the north-east coast of Canada. Such data is absolutely necessary in order to run the statistical model. It is also utilized to analyse the accuracy of both models. The result from the test runs will be used to further comment on the best method for prediction of short term iceberg drift. Uncertainty range of input fields will be estimated. Choice of important model parameters will be discussed, and an ensemble system will be established. The ensemble will be based on perturbation of some of the model parameters, and

of the forcing fields within defined uncertainty ranges.

1.3 Objectives

The general objective of this thesis is to perform an in-depth study of existing iceberg drift models. This includes a review of the theoretical basis for the statistical approach, and a survey of the driving forces guiding iceberg drift in deterministic models. This study will include a discussion on which forces play a significant role and which may be neglected, and describe how significant forces are accounted for in relevant models.

If it, through the study in this thesis, is possible to confirm the accuracy of the OpenBerg module it would be a large step closer to making this model operational.

The specific objective of the thesis is to review the implementation, and analyse the performance of the OpenBerg module. To analyse the performance, ensemble analysis will be utilized to estimate the distribution parameters of the predictions. Assuming a known distribution, these parameters can be used to estimate the probability of an iceberg being a given distance from the prediction.

In other words, the main research question to be answered in this thesis is whether either of the models implemented in the OpenBerg module are suited for operational use.

1.4 Structure of the Thesis

The thesis is divided into 6 chapters including the introduction.

Chapter 2 presents the dynamic and statistical theory behind iceberg drift modelling, and reviews the approaches in various existing models along the way.

Chapter 3 reviews the observation data and the forcing data sets utilized for testing the OpenBerg module.

The methodology is presented in chapter 4. In this chapter the specific models implemented in the OpenBerg module is discussed. In addition, the OpenDrift framework and the OpenBerg module is described in more detail, and the

methods used in the result analysis are presented.

In chapter 5 the results from the test runs and the analysis are summarized.

Chapter 6 summarizes the results, proposes some future work and presents a conclusion

2

Theory

In order to take action against hazardous icebergs, close to shipping lanes or well sites, forecasting of drift paths is necessary. Models that have been developed for this purpose fall into two main categories; deterministic models and statistical models.

Deterministic models relies on the governing dynamic equations for the various sources of forcing upon the iceberg. This approach is rather intuitive, and could be described as the combination of various forcing vectors to obtain a future position prediction. These kind of models are rather robust in terms of accuracy, given that the model input includes good forecasts of the local conditions. However, problems occur when the forecasts of the various forcing conditions is not accurate. Especially low frequency currents in the ocean are difficult to predict (Garrett, 1985). These currents are those due to mechanisms such as tides, large scale circulation and gyres. On time scales as short as 1-2 days or shorter these currents have a high variance, which makes them difficult to predict (Dijkstra and Ghil, 2005).

Due to the issues related to unpredictable forcing components, a statistical approach was proposed. This method extrapolates a drift path as a weighted sum of previously measured velocities. The major difference from the deterministic approach is that statistical models relies on previous measurements of velocity, rather than forcing components based on forecasts. This method will therefore avoid problems from erroneously predicted sources of forcing data.

Statistical models may allow for some use of deterministic components if the source of forcing is predictable. The statistical method employed by OpenBerg use deterministic prediction for forcing due to wind and tides, and extrapolates drift due to other sources based on previous velocities (this extrapolated *residual* component mainly consists of the forcing from the ocean current).

This chapter will present the theory behind the particular deterministic and statistical models employed by OpenBerg, as well as alternative existing models.

2.1 Definitions

Some terms that is useful to understand properly before reading this report is defined in this section.

Eulerian Flow Field This is a way of looking at fluid motion that focuses on specific locations in a space which the fluid flows through (Batchelor, 2000). A simple way of thinking of this is by sitting by the riverside and watching water pass your, fixed, location.

Lagrangian Flow Field This specification of the flow field is an approach to fluid motion where the observer follows one individual parcel of the fluid as it is displaced (Batchelor, 2000). A plot of the position for one individual parcel moving in time and space produces the path line of the parcel. This can be visualized similarly to the Eulerian field, but now as floating down a river at the same speed as the water.

Velocity Auto Correleation Function (ACF) The ACF is the function which describes the correlation between the velocity of an object at one point in time with a delayed copy of itself, as a function of the time delay. A Lagrangian version of the ACF is used in the statistical model in order to extrapolate future velocity.

The Ekman Depth The Ekman depth is the depth of the layer in a fluid where there is a force balance between pressure gradient force, Coriolis force and turbulent drag. And hence the top layer of the fluid where the surface drag plays no role.

Inertial Waves Inertial waves is a kind of internal wave which can be propagated in an incompressible, rotating fluid. These waves are due to the Coriolis force which occur in rotation. Inertial waves flow through the interior

of the fluid, not at the surface. And, since the Coriolis force do no work on the moving fluid, the energy in such waves is entirely kinetic (Landau and Lifshitz, 1987).

2.2 Dynamic Modelling of Iceberg Drift

When modelling the drift of any types of particles, icebergs are no different, the fundamental fluid dynamics are essential. In addition there are several external forcing components which are necessary to take into account, the various models weigh these different components differently. Some, as that of Wesche and Dierking (2016), models are constructed as to view the effects of a single forcing component.

In this section we will discuss the fluid dynamics briefly, and look closer at the various forcing components significant for iceberg drift. Along the way various approaches used in different models will be reviewed.

2.2.1 Fluid Dynamic Equation of Motion

The starting premise of geophysical fluid dynamics is that the dynamics of e.g. atmospheric and oceanographic motions are determined by the systematic application of the fluid continuum equations of motions (Pedlosky, 2013). The equations of motions and the Coriolis force are discussed in more detail in appendix A, but a brief outline is presented here.

To describe the motion, required dynamical variables are generally the density ρ, the pressure p, the velocity vector $\mathbf{u}$. To close the system to other variables we assume the condition of mass conservation to be valid, and constant density. The condition of mass conservation requires the absence of sources or sinks of mass in the fluid. It is formulated by the continuity equation, which is expressed as

$$\frac{\partial \rho}{\partial t} + \nabla \cdot \rho \mathbf{u} = 0, \tag{2.1}$$

where ∇ is the vectorial differential operator, and t is time. Equation 2.1 states that the local increase of density with time, must be balanced by a divergence of

the mass flux $\rho\mathbf{u}$. For constant density this condition can be simplified:

$$\nabla \cdot \mathbf{u} = 0. \tag{2.2}$$

If the density is not considered constant, one would have to consider thermodynamics to account for its variations. In relation to iceberg drift it is very reasonable to consider the density to be constant, and no additional variables are traditionally considered to be relevant.

For constant density, the system is closed such that we have four variables, p and $\mathbf{u} = (u, v, w)$. We need four equations to solve this system. One of equations is the continuity equation, derived in equation 2.2. The other three are the equations of motion in the three directions. The most natural frame from which to describe atmospheric and oceanic motions, is one which rotates with the Earth's angular frequency Ω, due to our perspective lining on the surface of the planet. From this frame of reference the momentum equation for a pocket of sea water can be expressed as (e.g. Pedlosky, 2013)

$$\rho\left[\frac{d\mathbf{u}}{dt} + f \times \mathbf{u}\right] = -\nabla p + \rho\nabla\Phi + \mathscr{F}, \tag{2.3}$$

where $\frac{d}{dt}$ is the time derivative, ∇ is the vectorial differential operator, and the non-conservative forces $\mathscr{F}$. Φ is the total potential, and accounts for potentials due to both conservative body forces (such as gravity), and the perceived potential due to the centripetal acceleration. f is the Coriolis parameter, it is a function of the latitude angle φ and can be expressed as

$$f = 2\Omega sin\varphi. \tag{2.4}$$

Equation 2.3 states that the mass per unit volume times the acceleration (from the rotating frame of reference) is equal to the sum of the pressure gradient force $-\nabla p$, the body force per unit mass $\rho\nabla\Phi$ and the non-conservative forces $\mathscr{F}$.

$\mathscr{F}$ may represent any non-conservative force, and is independent of the frame of reference. This term account for all external forcing. In the following section, it is discussed at length which forcing components are significant in iceberg modelling.

2.2.2 Forcing Components

External forcing components usually included by various existing models, are forces due to air drag $\mathbf{F}_a$, water drag $\mathbf{F}_w$, the water pressure gradient force $\mathbf{F}_p$, forces due to wave radiation stress $\mathbf{F}_r$, and the Coriolis force $f \times \mathbf{V}$. Where $\mathbf{V}$ is the velocity of the iceberg. Some models (e.g Kubat et al., 2005) include a term $\mathbf{F}_{am}$ accounting for the momentum of the wake formed behind the iceberg called *added mass*. Certain models also account for sea-ice drag, but drift within sea ice is not a problem of interest for this thesis and will not be discussed in detail.

A balance equation of linear momentum including all the components mentioned above may be expressed as (e.g Kubat et al., 2005)

$$m\left(\frac{d\mathbf{V}}{dt} + f \times \mathbf{V}\right) = \mathbf{F}_a + \mathbf{F}_w + \mathbf{F}_r + \mathbf{F}_p + \mathbf{F}_{am}. \tag{2.5}$$

The left hand side is similar to equation A.20 but now applied to a drifting iceberg of mass m, moving at velocity $\mathbf{V}$, and f is the Coriolis parameter.

Now let us take a closer look at the terms on the right hand side. The force due to air drag in its exact form can be expressed as (Smith, 1993)

$$\mathbf{F}_a = \frac{1}{2}\rho_a C_a A_a |\mathbf{V}_a - \mathbf{V}|(\mathbf{V}_a - \mathbf{V}), \tag{2.6}$$

where ρ_a is air density, C_a is the the non-dimensional air drag coefficient, A_a is the cross-sectional sail area, $\mathbf{V}_a$ is the wind velocity, and $\mathbf{V}$ is the iceberg velocity. The sail is the part of the iceberg above the waterline, as sketched in figure 2.1.

There are some dispute on how to take into account in the wind drag in a simple and accurate fashion. According to Smith (1993) the wind drag should always be proportional to the square of the relative wind velocity $(\mathbf{V}_a - \mathbf{V})$ (the difference between wind velocity and iceberg velocity). Garrett et al. (1985a) found, through cross-correlation of wind and iceberg velocity components, that the correlation between components in the same direction was consistent with the iceberg moving at a fraction of about 1.8% of the wind speed. However, it is commonly accepted that the drift velocity of an iceberg relative to the ocean current is at about 2% of the wind speed (e.g. Smith, 1993; Bigg et al., 1997). This fraction is so small that some, e.g. Kubat et al. (2005), for simplicity choose to replace the relative velocity by the wind velocity $\mathbf{V}_a$ itself.

In a similar way the force due to water drag can be expressed as

$$\mathbf{F}_w^1 = \frac{1}{2}\rho_w C_w A_w |\mathbf{V}_w - \mathbf{V}|(\mathbf{V}_w - \mathbf{V}), \tag{2.7}$$

where ρ_w is the water density, C_w is the non-dimensional coefficient for water drag and A_w denotes the cross sectional vertical area of the iceberg exposed to the water normal to the current (Gaskill and Rochester, 1984). $\mathbf{V}_w$ is the water current velocity vector. The superscript above $\mathbf{F}_w$ denotes the versions of this expression, as alternative versions will be presented below. For instance in the model presented by Kubat et al. (2005) the *keel* (the part of the iceberg below the water surface) is considered to consist of layers, each of 10 m depth. This model implements a modified version of equation 2.7

$$\mathbf{F}_w^2 = \frac{1}{2}\rho_w C_w \sum_k A_w(k) |\mathbf{u}_w(k) - \mathbf{V}|(\mathbf{u}_w(k) - \mathbf{V}), \tag{2.8}$$

where $A_w(k)$ is the vertical area of layer k, and $\mathbf{u}_w(k)$ is the water current acting on layer k. This description of the water drag allows us to use more complex, layered, forcing data to predict the drift. In Turnbull et al. (2015) the water drag is described similarly to how it is presented in Kubat et al. (2005), but another term is included in order to account for the drag along the bottom of the iceberg. The expression then is modified into a third version:

$$\mathbf{F}_w^3 = \mathbf{F}_w^2 + (\rho_w C_{dw} A_b) |\mathbf{u}_w - \mathbf{V}|(\mathbf{u}_w - \mathbf{V}), \tag{2.9}$$

where C_{dw} is the non-dimensional skin drag coefficient of water along the bottom surface of the iceberg, A_b is the horizontal area of the iceberg bottom and $\mathbf{u}_w$ is the ocean current velocity along the bottom horizontal surface.

When an iceberg is moving relative to stationary water is creates waves as the iceberg is pushing water out of the way. This force is called the wave radiation force. The forces acting on the iceberg due to this effect can be isolated and linearised. This simplification does, however, require the assumption that the forces due to interaction between the iceberg and the moving water flow is isolated from the wave radiation force (i.e. accounted for by other force components). Whereas the interaction between the iceberg and the stationary flow exclusively happens in the wave radiation force (Hover and Triantafyllou, 2009).

If the wave radiation force force is absorbed at a deep vertical wall, its magnitude is (Smith, 1993)

$$F_r = \frac{1}{4}\rho_w g a^2 L, \tag{2.10}$$

where g is the gravitational constant and L is the length of the iceberg normal to incident waves of amplitude a. This force represents an imperfect transfer of momentum between the waves and iceberg. It is relative to the shape of the iceberg, and is smaller for shapes that is not perfect reflectors. If the shape iceberg reflects the waves perfectly the magnitude of this force can be doubled. While waves with long wavelengths (wavelength greater than L) may pass without being reflected nor absorbed, and thereby having negligible effect on F_r. Using the assumptions that the expression in equation 2.10 is applicable to a moving iceberg and that this force works in the wind direction, the expression for the wave radiation force will be (Bigg et al., 1997)

$$\mathbf{F}_r^1 = \frac{1}{4}\rho_w g a^2 L \frac{\mathbf{V}_a}{|\mathbf{V}_a|}, \tag{2.11}$$

where the superscript above $\mathbf{F}_r$ denotes the version of the expression and $\mathbf{V}_a$ still is the wind velocity vector. Other proposed expressions for this force have been presented, where it is formulated as a perfect reflector but rather introduce a wave force coefficient C_{wf} (see for example Kubat et al., 2005; Carrieres et al., 2001). Where C_{wf} would not be constant, but rather depend on the iceberg length L in relation to ocean wavelength. The version presented in Carrieres et al. (2001) is on the form

$$\mathbf{F}_r^2 = \frac{1}{2}C_{wf}\rho_w g H^2 L \kappa, \tag{2.12}$$

where κ is the unit wave direction vector and H is the wave heigth ($H = 2a$). Carrieres et al. (2001) stresses that this term only accounts for *swell waves*, waves formed due to wind over extended periods of time (not created by local wind conditions), and not *wind waves* created by local wind. This is because it is assumed that equation 2.6 accounts for the effects of the wind waves. In Kubat et al. (2005) on the other hand it is accounted for the wind waves, in addition to swell waves, in the expression for the wave radiation force. It is

expressed on the form

$$\mathbf{F}_r^3 = \frac{1}{2} C_{wf} \rho_w g a^2 L |\mathbf{V}_a| \mathbf{V}_a. \tag{2.13}$$

In Kubat et al. (2005) it is assumed that, when implementing equation 2.13, the direction of the wind waves is the same as the wind direction. The direction of the swell waves will have to be provided as input to the model.

$\mathbf{F}_p$ denotes the pressure gradient force, and can be expressed in terms of the horizontal pressure field P (in the water), iceberg mass m and water density ρ_w such that

$$\mathbf{F}_p = -m \nabla P / \rho_w,$$

where ∇ is the horizontal pressure gradient. This term represents the forces acting upon an iceberg by the pocket of water surrounding it, and governed pressure gradients in the water at either side of the icebergs. These effects are created by tides, large scale circulation, gyres ect.. And in a sense this is the basic force creating motion in the water around the iceberg.

There are some small variations in different models in how they account for these forces. For instance the model presented in Kubat et al. (2005) expresses these forces in terms of the Coriolis parameter and the mean water flow, such that

$$\mathbf{F}_p^1 = m\left(\frac{d\mathbf{V}_{mw}}{dt} + f \times \mathbf{V}_{mw}\right), \tag{2.14}$$

where $\mathbf{V}_{mw}$ is the mean water current velocity for a given volume of water, and m is the iceberg mass. The superscript above $\mathbf{F}_p$ again denotes the version of the expression. This an expression for the sum of inertia and Coriolis forces on a volume of displaced water.

In Bigg et al. (1997) $\mathbf{F}_p$ is described by rearranging the equation for motion for $\mathbf{V}_{mw}$ (in terms of forces per unit mass):

$$\frac{d\mathbf{V}_{mw}}{dt} + f \times \mathbf{V}_{mw} = -\frac{1}{\rho} \nabla P + \frac{1}{\rho} \frac{\partial \tau}{\partial z}. \tag{2.15}$$

In equation 2.15, τ is the surface wind stress, and z is the vertical coordinate. In this approach the effects on $\mathbf{F}_p$ by surface wind stress is assumed to reduce to the product of the inverse Ekman depth E_k^{-1} (described in section 2.1) and the surface wind stress, atleast in practice. The surface wind stress can be expressed as (Gill, 1982)

$$\tau_s = 1.5 \times 10^{-3} \rho_a |\mathbf{V}_a| \mathbf{V}_a.$$

This results in the alternative expression for the pressure gradient force exerted on the iceberg

$$\mathbf{F}_p^2 = -m \frac{\nabla P}{\rho_w} + \frac{\tau_s}{E_k}, \tag{2.16}$$

where ρ_w is the water density and the Ekman depth is considered to be equal to the draft of the iceberg with a maximum value of 90 m (Bigg et al., 1997). The draft of an iceberg is visualized in figure 2.1.

There are some dispute about whether the ocean should be assumed to be in steady geostrophic equilibrium (e.g. Smith and Banke, 1983), which implies that the pressure force per unit mass on an iceberg is described solely by the term $f \times \mathbf{V}_{mw}$. Others (e.g. Bigg et al., 1996) argue that the dominant term in large oceanic regions is the material derivative $d\mathbf{V}_{mw}/dt$ (including non-linear advection terms), and that this term is the principal factor necessary to reproduce accurate iceberg drift distributions. In tropic regions the Coriolis parameter is small, which would effect which term is dominant. This is, however, not considered in any of the reviewed models as it is rare for icebergs to survive long enough for this effect to be relevant.

The wake of a drifting iceberg contains a large amount of water which is travelling at some fraction of the velocity of the iceberg. When the iceberg velocity changes a new wake is formed, and the momentum in this wake must be included in the force equations acting on the object. The observed effect of the water entrained in the wake, is that it adds to the mass of the drifting iceberg. In equation 2.5, $\mathbf{F}_{am}$ represents the force contribution from this added mass. In actuality it is accounted for by substituting the mass m in equation 2.5 by $(m + m_{am})$. m_{am} is the added mass and is assumed to be some ratio of them mass m. For instance Kubat et al. (2005) worked with an assumed added mass ratio of half the mass of the iceberg.

2.2.3 Iceberg Geometry

One major challenge for accurate trajectory prediction for icebergs is the ability to accurately describe the shape of the iceberg. For an operational model one must assume that in most cases the information about the shape and size of the iceberg is limited at best. In addition degradation of the iceberg over time and turnover (icebergs flipping upside-down) are problems that also makes the acquisition of accurate measurements more difficult.

The one measure of an iceberg which is generally easier to acquire than any other is the *waterline length*, which is defined as the largest horizontal distance across the iceberg at the waterline. An estimate of this measure is possible to determine from most data sources, be it from direct observation, aircraft photography or even satellite imagery. Barker et al. (2004) makes an attempt to describe the full geometry of an iceberg using only the waterline length, which Kubat et al. (2005) later implemented into their model.

Figure 2.1 visualizes the various terms utilized to describe the iceberg geometry to clarify the dimensions discussed. The *draft*, or *keel*, is defined as the part of the iceberg below the waterline. The *sail* is the part above the waterline.

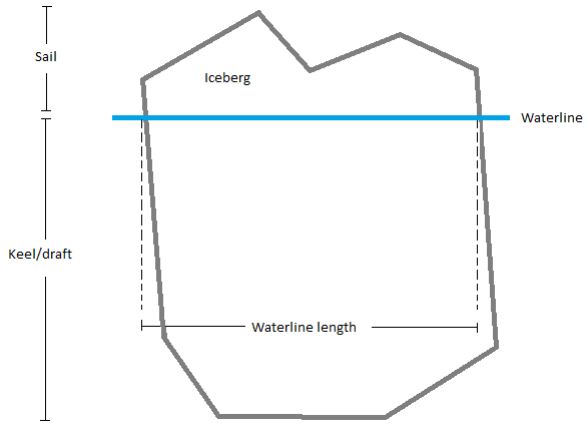

Figure 2.1: A simple sketch showing important terms used for describing iceberg geometry.

To find a relationship between waterline length L and the draft D of the iceberg, both measured in meters, Barker et al. (2004) curve-fitted measured dimension data. This data included height, length, width, draft, mass and cross-sectional area from several icebergs. They were able to find a relationship by fitting a power curve, similar to relationships presented in earlier works (e.g. Hotzel

and Miller, 1983; El-Tahan and Davis, 1985):

$$D = 2.91L^{0.71}. \tag{2.17}$$

However, an issue with this relation is that it includes dimensional parameters, and both the draft and waterline length parameters should be measured as a distance (meters). The power relation therefore does not accurately represent this relation. To avoid this problem, regression analysis was used instead. A dimensionless linear relationship was obtained to minimize the effects of erroneous data:

$$D = 0.7L. \tag{2.18}$$

Barker et al. (2004) account for the geometry of the iceberg draft by including into the model a set of parameters describing the keel geometry. These parameters are determined to fit a set of linear relations describing the keel-area of sections, where each section is of 10 m thickness. An expression for the cross-sectional area of the *sail* (the part of the iceberg above the water) is similarly described, but only by a single linear relation determined by input parameters.

The way the aforementioned parameters were determined by Barker et al. (2004), was by plotting waterline length versus cross-sectional area on available data. The relationship which best related the sail area A_s, observed in the data, to the waterline length was expressed as

$$A_s = a_0 L + b_0, \tag{2.19}$$

where a_0 and b_0 are the parameters determined by curve-fitting the data. Similarly, as the keel-area is split into vertical layers, each layer k needs an equation to describe the relation between the cross-section $A(k)$ and the waterline length. This can be expressed as

$$A(k) = a_k L + b_k, \tag{2.20}$$

where a_k and b_k are individual parameters for each layer of the keel.

A set of equations were originally developed for describing icebergs with drafts up to 160 m from a dataset where the largest measured draft was 120 m. All parameters were determined by curve-fitting available data. Later the equation parameters were improved upon by examining the relation between keel cross-sectional areas at adjacent depths. The result from this examination were the ability to produce simulated keel areas for keel depths of up to 200 m. The resulting equation parameters developed by Barker et al. (2004) are presented in table 2.1.

The OpenBerg software module, which is discussed in detail in chapter 4, applies the parameters in table 2.1 when estimating the draft used for deterministic trajectory modelling.

Table 2.1: Resulting parameters for calculating vertical cross-sectional areas from the studies of Barker et al. (2004). These parameters are used to create composite icebergs in the OpenBerg software module.

	Heigth/Depth (m)	a(k)	b(k)
Layer 1	0-10	9.5173	-25.94
Layer 2	10-20	11.1717	-107.50
Layer 3	20-30	12.4798	-232.01
Layer 4	30-40	13.6010	-344.60
Layer 5	40-50	14.3249	-456.57
Layer 6	50-60	13.7432	-433.33
Layer 7	60-70	13.4527	-519.56
Layer 8	70-80	15.7579	-1111.57
Layer 9	80-90	14.7259	-1125.00
Layer 10	90-100	11.8195	-852.90
Layer 11	100-110	11.3610	-931.48
Layer 12	110-120	10.9202	-1007.02
Layer 13	120-130	10.4966	-1079.62
Layer 14	130-140	10.0893	-1149.41
Layer 15	140-150	9.6979	-1216.49
Layer 16	150-160	9.3216	-1280.97
Layer 17	160-170	8.9600	-1342.95
Layer 18	170-180	8.6124	-1402.52
Layer 19	180-190	8.2783	-1459.78
Layer 20	190-200	7.9571	-1514.82

Using the equations defined by table 2.1 combined with the relation found in equation 2.18, composite icebergs can be created. Two examples of such composites are presented in figure 2.2.

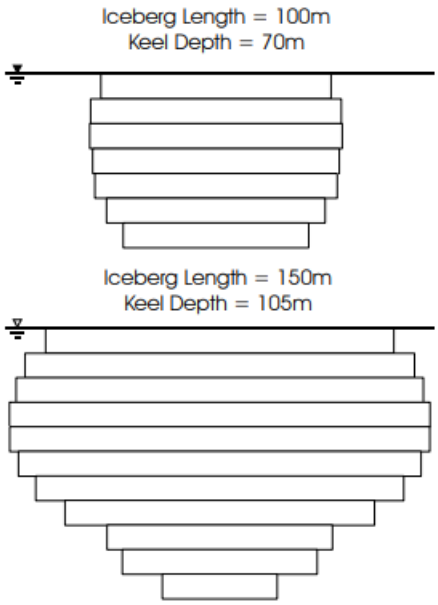

Figure 2.2: Composite icebergs, created using equations from table 2.1 (Barker et al., 2004).

2.2.4 A Numerical Solution

By calculating the forces in equation 2.5, the acceleration of the iceberg, **a**, is obtained as a function of time and velocity

$$\mathbf{a}(t, \mathbf{V}) = \frac{d\mathbf{V}}{dt}. \tag{2.21}$$

The integral of equation 2.21 can be solved numerically, and the solution produces the velocity of the iceberg. This velocity is used to update the iceberg position. Previous models have used the traditional (forward) Euler approach, which uses the value of the acceleration at time step i to proceed to the next step, $i + 1$. However, this could lead to unstable solutions (especially if the size of the time steps is large). Therefore it is suggested by Kubat et al. (2005) an implicit Euler approach, also known as the backward Euler approach. In this method the acceleration at the next time step, $i + 1$, is estimated in advance and used to update the velocities. This results in a solution which is stable for relatively large time steps.

The form of the implicit Euler approach, based on equation 2.21, is

$$\mathbf{V}_{i+1} = \mathbf{V}_i + \mathbf{a}_i(t_{i+1}, \mathbf{V}_{i+1})\Delta t \tag{2.22}$$

where the subscripts denotes time steps (see for example Press et al. (1989)). This expression is used to compute the approximation of the future velocity. It can be further linearized using a first-order Taylor expansion of $\mathbf{a}$ around $\mathbf{V}_i$:

$$\mathbf{V}_{i+1} = \mathbf{V}_i + \Delta t \left[\mathbf{a}_i(t_{i+1}, \mathbf{V}_i) + \left. \frac{\partial \mathbf{a}}{\partial \mathbf{V}} \right|_{V_i} (\mathbf{V}_{i+1} - \mathbf{V}_i) \right] \tag{2.23}$$

Where $\frac{\partial \mathbf{a}}{\partial \mathbf{V}}$ is a matrix of partial derivatives, the element includes the water drag and the Coriolis force term from 2.5. By solving equation 2.23 we obtain the velocity components for time step $i + 1$, given solely by values at time step i (Kubat et al., 2005)

$$\mathbf{V}_{i+1} = \mathbf{V}_i + \Delta t \left[\mathbb{I} - \Delta t \frac{\partial \mathbf{a}}{\partial \mathbf{V}} \right]^{-1} \mathbf{a}_i, \tag{2.24}$$

Where $\mathbb{I}$ is the identity matrix, and $\left[\mathbb{I} - \Delta t \frac{\partial \mathbf{a}}{\partial \mathbf{V}} \right]$ is a matrix from which we can obtain the velocity components by inversion.

2.2.5 Experiences With Dynamic Iceberg Modelling

The results from the studies of Kubat et al. (2005) serves as a good introduction, and provides an overview of earlier modelling studies. They ran tests of their model by simulating drift tracks to ensure accuracy, and by performing a parametric study by examining changes of predicted tracks to varying input parameters and environmental forces. Their results showed that:

- Water current has the most pronounced effect on the forecast. Using the vertical profile of water current provided the best agreement between predicted and observed tracks. Employing a current averaged over the iceberg's keel depth yielded smaller errors than detailed water current

vertical profiles. However, using surface current values only, led to significant errors.

- The waterline length does also have a strong influence on the drift predictions. This result was not surprising as this parameter was used to calculate both the mass of the iceberg and the keel cross-sectional area. The results showed that using a value between the mean of the length and width (largest and smallest dimensions at the waterline) and the largest dimension at waterline, gave the best fit with observed track. How to determine the best estimates of the waterline variable requires more work according to Kubat et al. (2005).

- Waves might have a pronounced role in some cases. However, the data used for testing did not include measurements for wave conditions. Some tests were run considering wind waves with values for wave height within a reasonable range. The test showed that heights below 0.5 m did not have prominent effect on the predicted track, but as wave height increased above 0.5 m, the effects became more pronounced. Unfortunately the lack of data impeded the ability to draw proper conclusions about the effects of wave height.

- Water and air drag coefficients had little effect on the predictions. Tests showed that the icebergs drift path closely followed the mean water current (averaged over keel depth). As such, the relative velocity between the iceberg and water current is usually small, which indicates that the value of water drag coefficients have limited effect on the drift.

Advantages in dynamic models include:

- The dynamic models does not require any knowledge about the iceberg velocity to be able to predict the future trajectory. If an iceberg is observed the model can predict the future position based only on input data describing the surrounding forcing fields.

- With good estimates of parameters and good measurement and forecast values for environmental factors, Kubat et al. (2005) found their model to be reasonably accurate on time scales between 48 and 64 hours.

- Dynamic modelling allows for analysis of which forcing factors are most important for prediction of iceberg drift tracks.

Drawbacks in dynamic models include:

- The model is heavily impacted by the accuracy and availability of forecasts

from atmosphere, ocean and wave models. Inaccuracies in these models will in turn deteriorate the drift predictions.

- The problem of accurately representing the iceberg's geometry is challenging. Even using the waterline length L to estimate it, as described above, proves to be difficult. It is not easy to determine which representation of L provides the most accurate prediction tracks. Whether the description of the geometry is actually important is an interesting question, and a sensitivity study of this parameter was performed as a part of the research in this thesis.

2.3 Statistical Forecasting of Iceberg Drift

Statistical forecasting of iceberg drift bases the prediction of future position mainly on measured data of previous iceberg motions. This approach has also been dubbed *time series modelling* by some authors (e.g. Moore, 1985). The predictions produced are in the form of relative probabilities of possible trajectories. Therefore this approach needs only actually measured data to generate the model, thereby avoiding the problems regarding unpredictable input parameters in the deterministic approach. The underlying dynamics of the model do not directly enter into the computations, instead the input information is derived from the spatial and temporal correlations of recent and historical movements of the iceberg.

This section will take an in-depth look at a statistical approach attempting to create an optimum model where the future velocity of an iceberg is a weighted sum of previous velocities. The theory presented here is based heavily on the model presented by Garrett (1985).

2.3.1 Prediction Using Minimum Square Error as Criteria

First, we restrict ourselves to a single component of the velocity $u(t)$, for modelling. The goal is to develop a model predicting this variable using previous (observed) velocities of the iceberg. The best estimate $\hat{u}(t)$ of a future value can be estimated from a linear combination of the N previous velocity steps u_n where $n = 1, \ldots, N$, and each step is weighted by a parameter α_n (Garrett,

1985):

$$\hat{u}(t) = \sum_{n=1}^{N} \alpha_n u_n. \tag{2.25}$$

One will be able to predicate this future value in continuous time, as the weights can be estimated as continuous functions in time. More details about the weights are discussed in section 2.3.2 and 2.3.4.

What the "best" estimate actually is, depends on how we determine the criterion. The approach presented here defines the best estimate as the one which minimizes the mean square error (MSE) across several iterations, using the formula in equation 2.25. The error will in this particular case be defined as the difference between measured velocity u, and estimated velocity $\hat{u}$. The MSE can then be defined (Garrett, 1985):

$$e = \overline{[u(t) - \hat{u}(t)]^2} = \overline{[u(t)]^2} - 2\sum_{n=1}^{N} \alpha_n \overline{u(t)u_n} + \sum_{n=1}^{N}\sum_{m=1}^{N} \alpha_n \alpha_m \overline{u_n u_m}. \tag{2.26}$$

From equations 2.25 and 2.26 it is a well known result (the Gauss-Markov theorem) that the coefficients α_n can be obtained from the set of simultaneous equations

$$\sum_{m} \overline{u_n u_m} \alpha_m = \overline{u(t)u_n} \tag{2.27}$$

found by minimizing the MSE with respect to α_n (detailed proof for Gauss-Markov is available in e.g. Davis (1977)). The Gauss-Markov theorem also lets us rewrite the MSE as

$$e = [\overline{u(t)}]^2 - \sum_{n}\sum_{m} (Cov^{-1})_{nm} [\overline{u(t)u_n}][\overline{u(t)u_m}] \tag{2.28}$$

where Cov is the N by M covariance matrix with elements $\overline{u_n u_m}$, and $(Cov^{-1})_{nm}$ is element (n, m) of the inverse of Cov (Garrett, 1985).

The covariance vector, $\overline{u(t)u_n}$, and the covariance matrix are in general the values of the auto covariance at a certain time lag for the velocity values for a single iceberg trajectory.

Provided that the collected data is adequate to compute these covariances, this approach could in principle be implemented to predict future velocity which in turn can be used to predict future positions of an iceberg.

2.3.2 Prediction for an Exponentially Decaying Lagrangian ACF

Garrett (1985) assumed the drift to be a stationary process, such that u will also be stationary. The legitimacy of this assumption is debatable as the drift can only be considered stationary for short periods of time. Just how long this period is needs more extensive research. This thesis is testing the prediction capabilities of the OpenBerg module for iceberg trajectories on periods of up to 48 hours.

To estimate the weights, α_n, in equation 2.25, a useful tool is the the velocity ACF. We will consider the inputs u_n, the values of u at different times. Further we assume variance $\overline{u^2}$, and the ACF (Garrett, 1985)

$$R(\tau) = \frac{\overline{u(t)u(t+\tau)}}{\overline{u^2}}.$$

If we consider the values of u at times $-t_1$, $-t_2$, $-t_3$,..., the set of equations from equation 2.27 can be expressed as the matrix product:

$$\begin{bmatrix} 1 & R(t_2-t_1) & R(t_3-t_1) & \dots \\ R(t_1-t_2) & 1 & R(t_3-t_2) & \dots \\ \vdots & \vdots & & \end{bmatrix} \begin{bmatrix} \alpha_1 \\ \alpha_2 \\ \vdots \end{bmatrix} = \begin{bmatrix} R(t+t_1) \\ R(t+t_2) \\ \vdots \end{bmatrix}. \tag{2.29}$$

Now recall that for a real stationary process $R(\tau) = R(-\tau)$, such that e.g. $e^{-\gamma(t_1-t_2)} = e^{-\gamma(t_2-t_1)}$. Then assume that the ACF is exponentially decaying in time, and substitute for $R(\tau) = e^{-\gamma\tau}$ such that this product becomes

$$\begin{bmatrix} 1 & e^{-\gamma(t_2-t_1)} & e^{-\gamma(t_3-t_1)} & \dots \\ e^{-\gamma(t_2-t_1)} & 1 & e^{-\gamma(t_3-t_2)} & \dots \\ \vdots & \vdots & & \end{bmatrix} \begin{bmatrix} \alpha_1 \\ \alpha_2 \\ \vdots \end{bmatrix} = \begin{bmatrix} e^{-\gamma(t+t_1)} \\ e^{-\gamma(t+t_2)} \\ \vdots \end{bmatrix}.$$

$$= e^{-\gamma(t+t_1)} \begin{bmatrix} 1 \\ e^{-\gamma(t_2-t_1)} \\ \vdots \end{bmatrix}. \tag{2.30}$$

Which has the quite simple solution

$$\alpha_1 = e^{-\gamma(t+t_1)}, \alpha_2 = \alpha_3 = \cdots = 0. \tag{2.31}$$

This mean that the best prediction for the change in velocity at time $t + t_1$, is that measurement times the ACF at time lag $t + t_1$. It also implies that earlier velocity measurements do not provide any extra information. For large time changes this implies that the best prediction for velocity change is zero. Therefore the best statistical prediction of total velocity for large time changes will be the mean of past samples(Garrett, 1985).

2.3.3 Prediction of Position

Previously the inputs $u(-t_1), u(-t_2), \ldots,$ ect. was considered. Moving on we will consider how to obtain the predicted position by evaluating the output (Garrett, 1985):

$$x(t) = \int_0^t u(t')dt'. \tag{2.32}$$

To evaluate the reliability of the model, the root mean square error of the velocity estimate could be considered before calculating the predicted position. But there are, as we will see below, no guarantee that the best estimate for the velocity will produce the best estimate for the position.

To obtain the optimum predictor of position, $\hat{x}(t)$, (rather than the optimum predictor of velocity) using equation 2.32, we must retain the left side of equation 2.27 while replacing the right hand side, $\overline{u(t)u_n}$, by (Garrett, 1985)

$$\overline{x(t)u_n} = \overline{u^2} \int_0^t R(t' + t_n)dt' = \overline{u^2} \int_{t_n}^{t+t_n} R(\tau)d\tau. \tag{2.33}$$

The value of $\hat{x}(t)$, obtained by solving this integral, is the same as the value obtained by integrating the best estimate of $u(t)$ at each instant. If we solve equation 2.33 for $R(\tau) = e^{-\gamma\tau}$ we get

$$\overline{x(t)u_n} = \overline{u^2}\left(\gamma^{-1}(1 - e^{-\gamma\tau})e^{-\gamma t_n}\right). \tag{2.34}$$

Next the optimum estimate of position is obtained by using only the most recent

velocity estimate. Taking the most recent time estimate at $t_1 = 0$, equation 2.34 becomes

$$\hat{x}(t) = \gamma^{-1}(1 - e^{-\gamma t})u(0). \tag{2.35}$$

Combining equation 2.32 and the estimate in equation 2.35, the root mean square error (RMSE) for the position estimate is (Garrett, 1985)

$$RMSE = \sqrt{\overline{(x(t) - \hat{x}(t))^2}} = \sqrt{\overline{u^2}}\gamma^{-1} f(\gamma t), \tag{2.36}$$

where

$$f(\gamma t) = (2\gamma t - 3 + 4e^{-\gamma t} - e^{-2\gamma t})^{\frac{1}{2}}. \tag{2.37}$$

Note that the root mean square error for the position is proportional to the velocity fluctuation and decay time and will vary in time only due to the factor $f(\gamma t)$. For small time intervals, $\gamma t \ll 1$, this implies small growth in error, but for large time intervals, $\gamma t \gg 1$, the position error will behave like the fluid dynamical equivalent of a random walk (Taylor, 1922).

If we take the RMSE when no prediction is made (i.e. $\hat{x}(t) = 0$), f becomes

$$f_0(\gamma t) = (2(\gamma t - 1 + e^{-\gamma t})^{\frac{1}{2}}. \tag{2.38}$$

This function will behave as γt for $\gamma t \ll 1$, and as a random walk for $\gamma t \gg 1$.

Figure 2.3 show a plot of $f(\gamma t)$ and $f_0(\gamma t)$, i.e. perfect prediction and no prediction respectively. Graph (a) and (b) both display the same functions, but on different intervals, as to describe the change in behaviour for different scales of γt. Comparing the two plots show how the error in the perfect predictor ($f(\gamma t)$) behaves, compared to no prediction ($f_0(\gamma t)$), for different time scales.

This implies that the statistical method can be useful for short term prediction, but that the loss of memory will eventually lead to a large accumulation of errors such that even the best possible prediction is hardly better than no prediction at all (Garrett, 1985).

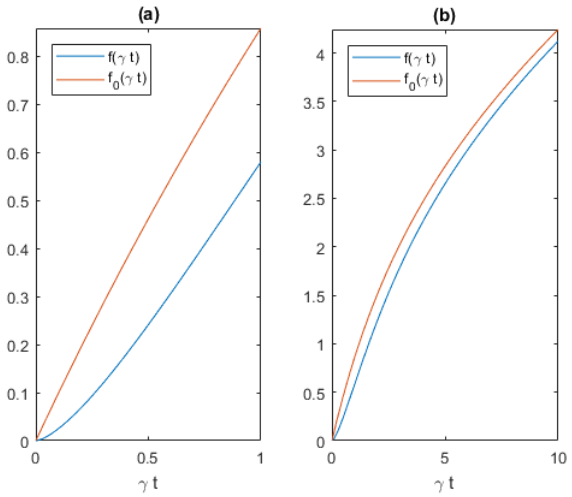

Figure 2.3: Both plots (a) and (b) show $f(\gamma t)$ and $f_0(\gamma t)$ from equations 2.37 and 2.38. The curves show the behaviour of the RMSE in the optimum prediction (f), versus no prediction at all (f_0). Plot (a) is of interval $[0, 1]$ and plot (b) of interval $[0, 10]$.

2.3.4 The Effect of Noise

Garrett (1985) found that effects of noise in the observational velocity data complicated the prediction scheme. In the presence of noise, the ACF behaved more like $R(\tau) = Ae^{-\gamma\tau}$ for $\tau > 0$, where A is a noise constant ($R(0)$ is naturally still equal to 1). To account for these effects the one-dimensional model above needs to be expanded.

We want to obtain optimum prediction of position

$$\hat{x}(t) = \sum_{n=1}^{N} \alpha_n u(-t_n), \tag{2.39}$$

given the ACF, $R(\tau) = Ae^{-\gamma\tau}$. This leads to the set of equations

$$\sum_{m=1}^{N} R(|t_m - t_n|)\alpha_m = \int_0^t R(t' + t_n)dt', \tag{2.40}$$

where the coefficients α_m are functions of time.

Before the ACF was assumed to be $R(\tau) = e^{-\gamma\tau}$, and the coefficients α_n were

determined to be

$$\alpha_1 = e^{-\gamma(t+t_1)}, \alpha_2 = \alpha_3 = \cdots = 0.$$

This implied that the the number of steps used for prediction did not matter. As we will see, this is no longer the case.

In the modified ACF, the measure of noise A is a constant smaller than 1 and decreases as the noise increases. Recall that $R(0) = 1$, then if every t_n is separated by one time unit we obtain new coefficients expressed as

$$\alpha_n = A\gamma_n^{-1} e^{-\gamma t_1}(1 - e^{-\gamma t})\beta_n, \tag{2.41}$$

corresponding to (Garrett, 1985)

$$\begin{bmatrix} 1 & Ae^{-\gamma} & Ae^{-2\gamma} & \dots \\ Ae^{-\gamma} & 1 & Ae^{-\gamma} & \dots \\ \vdots & \vdots & & \end{bmatrix} \begin{bmatrix} \beta_1 \\ \beta_2 \\ \vdots \end{bmatrix} = \begin{bmatrix} 1 \\ e^{-\gamma} \\ \vdots \end{bmatrix}. \tag{2.42}$$

In the limit $A = 1$ this corresponds to the noise-free instance, and equation 2.42 implies $\beta_1 = 1, \beta_2 = \beta_3 = \cdots = 0$. In the other limit, $A \to 0$, we get $\beta_1 = 1, \beta_2 = e^{-\gamma}, \dots$. This case is not of interest as it means that the data would be completely distorted by noise, and no sensible prediction would be possible to make.

In the interval $0 < A < 1$ the solution to equation 2.42 cannot be expressed as a linear combinations of the two solutions in the limits. However, as A decreases it is clear that the significance of weights other than α_1 increases. To analyse the effects of noise in the model it is useful to look at the mean square position error normalized by the mean square speed. For an AFC $R(\tau)$, the normalized error e is

$$e(t) = \frac{\overline{(x(t) - \hat{x}(t)^2}}{\overline{u^2}} = 2\int_0^t \int_0^{t'} R(t'')dt''dt' - \sum_{n=1}^{N} \alpha_n \int_0^t R(t' + t_n)dt'. \tag{2.43}$$

Accounting for the presence of noise (equations 2.41 and 2.42), this expression

can be modified to

$$\gamma\sqrt{\frac{e(t)}{A}} = \sqrt{2(\gamma t - 1 + e^{-\gamma t}) - A(1 - e^{-\gamma t})^2 e^{-\gamma t_1} \sum_{n=1}^{N} \beta_n e^{-\gamma t} n}. \tag{2.44}$$

By introducing the noise term s the error is increased, because the trajectory is less predictable. But it is also reduced, due to that no more than a fraction A of the total variance is associated with persistent and diffusive ocean currents(Garrett, 1985).

The optimum prediction using this scheme will only be obtained when $N \longrightarrow \infty$. Figure 2.4 is a graphical representation of the RMSE for various values of N, compared to the RMSE for the perfect prediction and no prediction shown in figure 2.3. Garrett (1985) argues that noise significantly increases the error of the optimum prediction, but that it converges towards the limit value by the time N is about 10. It is also suggested by Garrett (1985) that the RMSE is not significantly greater than the limiting value (at $N \longrightarrow \infty$) for $N = 1$.

Therefore Garrett (1985) suggests to retain the one-term prediction scheme, but one where the weight α_1 is reduced using equations 2.42 and 2.41, with parameters suitable for the noise level. Failure to reduce the weight does not degrade the prediction seriously at low noise levels, but for high noise levels failure to do so can lead to predictions worse than that of the random walk.

2.3.5 Two Dimensional Model

One way to allow for modelling in two dimensional (2D) is to use complex numbers to account for the two components of motion. We denote the complex velocity $w = u + iv$, and the position $z = x + iy$. The prediction for 2D can be expressed as the linear combination

$$\hat{z}(t) = \sum_{n=1}^{N} \alpha_n w_n, \tag{2.45}$$

where α_n are complex coefficients. w_n is the observed velocity in the N-th velocity step previous to the time of the prediction, which can be denoted $w_n = w(-t_n)$.

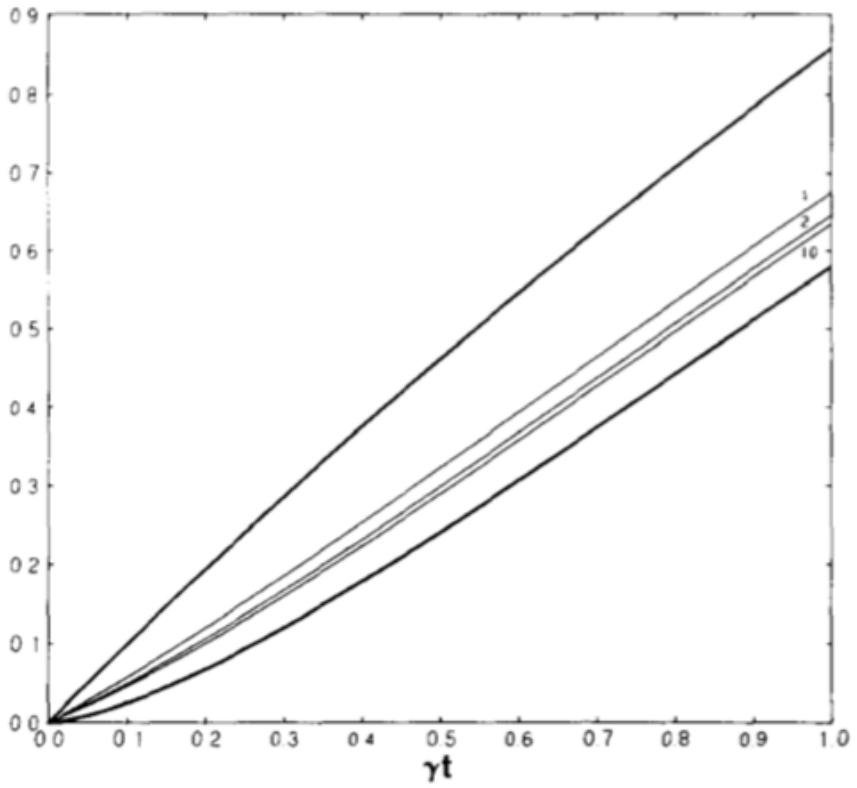

Figure 2.4: Plot that show the scaled RMSE of the position for noisy data, from equation 2.44, as thin lines. It also includes $f(\gamma t)$ and $f_0(\gamma t)$ from figure 2.3 as the thicker lines. The RMSE for the noisy data are plotted with $A = 0.7$ and $\gamma = \frac{1}{15}$ for three different values of N, N=1,2,10. Figure is adapted from Garrett (1985), page 261.

We seek the complex coefficients which minimizes the mean position error. The position error may be expressed in terms of z or in terms of x and y:

$$\textit{Mean position error} = \overline{(z-\hat{z})(z^*-\hat{z}^*)} = \overline{(x-\hat{x})^2+(y-\hat{y})^2},$$

where '$*$' denotes the complex conjugate. To determine the complex coefficients, we obtain a set of equations (corresponding to equation 2.40) (Garrett, 1985)

$$\sum_{m=1}^{N} W^*(t_m - t_n)\alpha_m = \int_0^t W(t'+t_n)dt', \tag{2.46}$$

where

$$W(\tau) = R(\tau) + iC(\tau). \tag{2.47}$$

with $R(\tau)$ defined as the ACF for either u or v, and $C(\tau)$ defined as the cross-correlation function $\overline{u(t)v(t+\tau)}$:

$$R(\tau) = \overline{u(t)u(t+\tau)} \text{ or } R(\tau) = \overline{v(t)v(t+\tau)}$$

$$C(\tau) = \overline{u(t)v(t+\tau)}$$

We have (in equation 2.46) assumed that the mean square speed is equal in the two directions ($\overline{u^2} = \overline{v^2}$).

Now the normalized mean square position error can be extended into 2D, expressed as (Garrett, 1984)

$$e(t) = \frac{[\overline{(x-\hat{x})^2+(y-\hat{y})^2}]}{2\overline{u^2}} = 2\int_0^t \int_0^{t'} R(t'')dt''dt' - \sum_{n=1}^{N} \alpha_n \int_0^t W^*(t'-t_n)dt'. \tag{2.48}$$

Inertial Waves

Before we try to solve equation 2.46 let us discuss an implication of the 2D extension. It allows for inclusion of inertial waves into the model. The velocity vector of the inertial waves rotates clockwise with the Coriolis frequency (Coriolis parameter), f. Note that due to the properties of the ACF and the cross-correlation function we know that:

$$R(\tau) = R(-\tau),$$

$$R(0) = 1,$$

$$C(-\tau) = -C(\tau)$$

and,

$$C(0) = 0$$

This implies $C(\tau) < 0$ for a small and positive τ. Now we can extend the model, if we remember that $R(0) = 1$, we obtain for $\tau \neq 0$ (Garrett, 1985)

$$W(\tau) = A_1 e^{-\gamma_1|\tau|} + A_2 e^{-\gamma_2|\tau|} e^{if\tau} \tag{2.49}$$

The first term in equation 2.49 accounts for the isotropic, non-rotating, low frequency motions. While the second term accounts for the inertial wave. The decay term $e^{-\gamma_2|\tau|}$ allows for finite bandwidth and decorrelation of the inertial waves across a time $-\gamma_2^{-1}$.

The factors A_1 and A_2 account for the noise level. $A_1 + A_2 = 1$ implies no noise, while $A_1 + A_2 < 1$ implies the presence of noise (Garrett, 1985).

Solving the 2D Model

Now we move on to determining the 2D parameters. The solution to the set of equations 2.46 may be written as (Garrett, 1985)

$$\underline{\boldsymbol{\alpha}} = \underline{\boldsymbol{\alpha}}_1 + \underline{\boldsymbol{\alpha}}_2 \tag{2.50}$$

with

$$\underline{\boldsymbol{\alpha}}_1 = A_1\gamma_1^{-1}(1 - e^{-\gamma_1 t})e^{-\gamma_1 t_1}\underline{\boldsymbol{\beta}}_1 \tag{2.51}$$

and

$$\underline{\boldsymbol{\alpha}}_2 = A_2(\gamma_2 - if)^{-1}[1 - e^{-(\gamma_2+if)t}] \times e^{-(\gamma_2+if)t_1}\underline{\boldsymbol{\beta}}_2 \tag{2.52}$$

The two coefficients $\underline{\boldsymbol{\beta}}_1$ and $\underline{\boldsymbol{\beta}}_2$ must for

$$\boldsymbol{M} = \begin{bmatrix} 1 & A_e^{-\gamma_1} + A_2 e^{-(\gamma_2 - if)} & \dots \\ A_e^{-\gamma_1} + A_2 e^{-(\gamma_2+if)} & 1 & \dots \\ \vdots & \vdots & \end{bmatrix} \tag{2.53}$$

satisfy

$$\boldsymbol{M}\underline{\boldsymbol{\beta}}_1 = \begin{bmatrix} 1 \\ e^{-\gamma_1} \\ \vdots \end{bmatrix} \tag{2.54}$$

and

$$\boldsymbol{M}\underline{\boldsymbol{\beta}}_2 = \begin{bmatrix} 1 \\ e^{(\gamma_2+if)} \\ \vdots \end{bmatrix} \tag{2.55}$$

For different values of the parameters A_1, A_2, γ_1, γ_2 and N, equations 2.54 and 2.55 are solvable for $\underline{\boldsymbol{\beta}}_1$ and $\underline{\boldsymbol{\beta}}_2$. These solutions can be used to evaluate the error defined in equation 2.48. It is argued by Garrett (1985) that (as before) the RMSE was not significantly reduced for N more than one, and it is recommended to stick to the one-term prediction scheme.

Further analysis of the RMSE using various values for the parameters, and even choosing noise parameters that are slightly off from the true value of the process in question, leads Garrett (1985) to conclude that the single-term predictor is fairly robust.

2.3.6 Confidence Limits

Assuming that the RMSE for the position (i.e. variance) may be calculated, and that it has some error distribution, a confidence limit for the prediction may be acquired. The probability, $P(d)$, of an iceberg being a distance r' from the predicted position may be calculated from the assumed distribution (usually Gaussian). Given a probability p that a circle of radius r around the predicted position contains the iceberg we have that

$$\int_0^r P(r')dr' \tag{2.56}$$

And a confidence limit, for any chosen p, for the iceberg position may be acquired by solving equation 2.56 for r.

2.3.7 An Overview of Statistical Iceberg Modelling

The statistical model presented in this chapter allows for predictions of iceberg trajectories based on initial velocities, while also accounting for inertial oscillations (assuming the process is stationary). It will at any instant provide a predicted trajectory and, assuming isotropy, a circle about particular points of interest where the radius is describing a particular confidence interval.

An example of a prediction is displayed in figure 2.5. In this example mean tides and inertial waves are ignored, and a one-term predictor is used for implementation. The predictions are made with prediction intervals of one hour. Parameter values are chosen by Garrett (1985) based on analysis of a data set from The Labrador shelf (off the east coast of Canada).

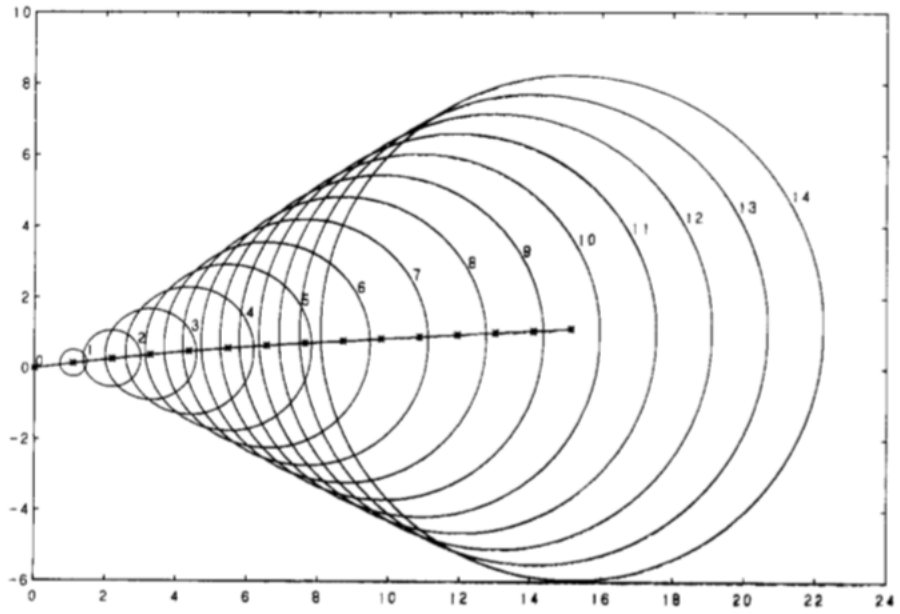

Figure 2.5: Predicted drift trajectory and circles of radius equal to the RMSE for position. Initial velocity for the track was $(0.0, 0.05)ms^{-1}$ with $A_1 = 0.7$, $A_2 = 0.1$, $\gamma_1^{-1} = \gamma_2^{-1} = 15h$ and $\overline{(u')^2} + \overline{(v')^2} = 0.06m^2s^{-2}$ for the total mean velocity including noise. This case use the one term predictor and a mean flow of $(0.3, 0.0)ms^{-1}$. The distance is measured in kilometres. The figure is adapted from Garrett (1985), page 264.

Advantages in statistical models include:

- It does not call for an extensive data set when predicting the future trajectory of an iceberg, as prediction using $N > 1$ does not significantly reduce the error.
- It is robust to slight mistakes in the estimation of its parameter.
- Simplicity of implementation and calculation of the scheme.

Drawbacks in statistical models include:

- A finite decorrelation time. For any statistical prediction where the decorrelation is finite, the error soon becomes rather large. This implies that the model will only be reliable for short term predictions.
- For cases with relatively small mean flow, circles marking the bounds of the confidence limits can grow upstream relative to the mean flow. This

makes it possible for the model to increase the chances of collision with a certain target, even after the the mean flow has carried the iceberg past the target.

3

Data Set

This chapter will discuss the data used to run and test the OpenBerg module. The observed iceberg tracks used in this thesis were kindly provided by Dr. Luke Copeland. Dr. Copeland is a Professor and University Research Chair in Glaciology of the Department of Geography, Environment and Geomatics, at the University of Ottawa (UO). The data consisted of GPS tracking data of several icebergs which calved in the Baffin Bay during the late summer of 2016.

To produce drift forecasts using the OpenBerg dynamic model and statistical-plus model, forcing data was needed. Current data was taken from the Regional Ice Ocean Prediction System (RIOPS) data set, accessed via the THREDDS-server connected to the open source portal *Ocean Navigator*. The wind data used was from from the European Reanalysis 5 (ERA5) data set, produced by the *European Centre for Medium-Range Weather Forecasts*, accessed using the Climate Data Interface (CDI). In addition, tidal current data was generated for each track using the WebTide model distributed by *the Bedford Institute of Oceanography*.

3.1 The 2016 Baffin Bay Data Set

The observation data provided for use in this thesis originates from nine different icebergs drifting in Baffin Bay. The tracks were obtained utilizing

deployed beacons with Iridium-connected RockSTAR GPS trackers that transmit their position hourly. The GPS beacons were deployed in the summer of 2016 and each track transmitted data over periods from a few weeks up to several months, with some drifts of more than 1000 km. All tracks are plotted in figure 3.1.

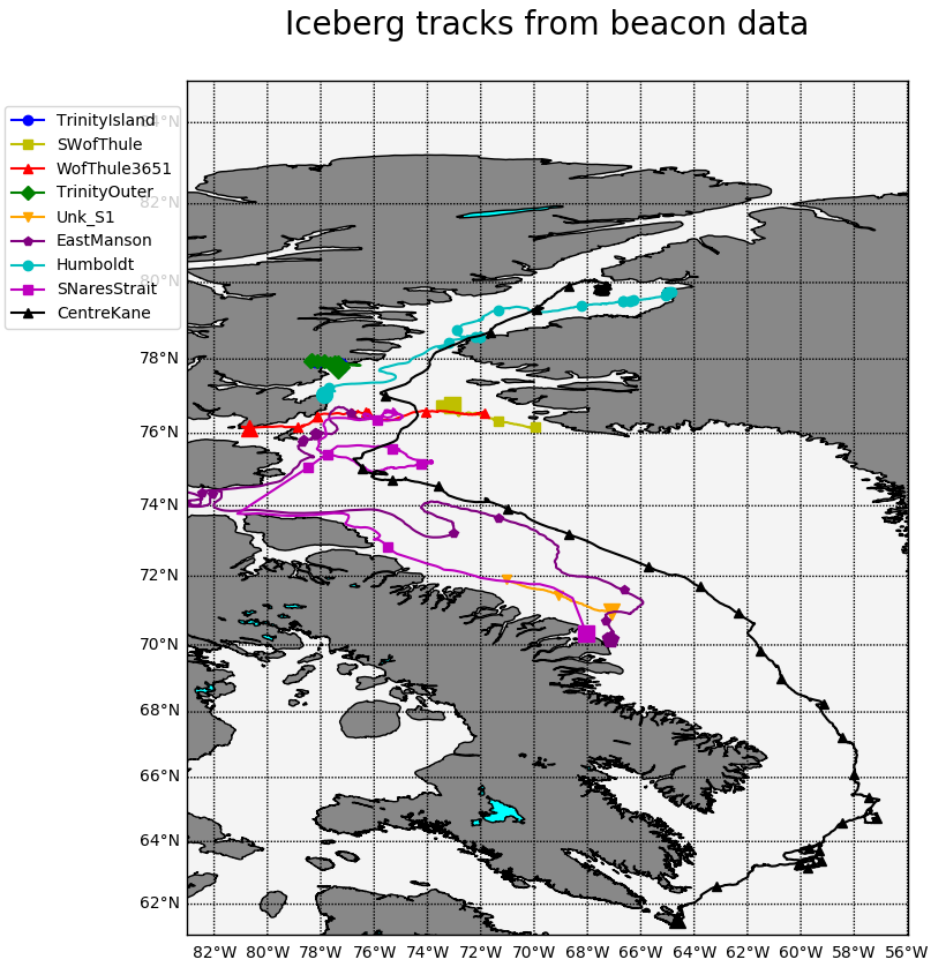

Figure 3.1: Plot of the observed tracks for all icebergs in the Baffin Bay data set. The end point of each track is represented by a larger marker.

In addition to the tracking data the set included extensive photos of each iceberg. For the analysis part of this thesis a subsection of one particular track was isolated and utilized. Figure 3.2 show a picture of the selected iceberg which is labelled *S Nares Strait*.

Figure 3.2: Image taken of the iceberg labelled *SNaresStrait* on the day the GPS beacon was deployed. Image courtesy: Luke Copeland UO.

Unfortunately, due to the use of helicopter to deploy the tracker it was difficult to take images with a proper perspective to get a sense of the size of the iceberg. The picture taken from the surface of the same iceberg is shown in figure 3.3, helps give some perspective.

3.1.1 Observed Trajectories

The OpenBerg module was initially constructed by Ron Saper to suit data consisting of tracks from 2012 in the vicinity of the *Hibernia GBS* (a large offshore oil-platform). This data was based on surface radar tracks collected by Provincial Air Lines, and are encoded in text files containing a series of timestamps with associated latitudes and longitudes. The Baffin Bay data was provided in CSV-format, which unfortunately was not a format that the module instantly could read. However, it proved to be quite trivial to modify the data into suitable text files using built in tools in Windows.

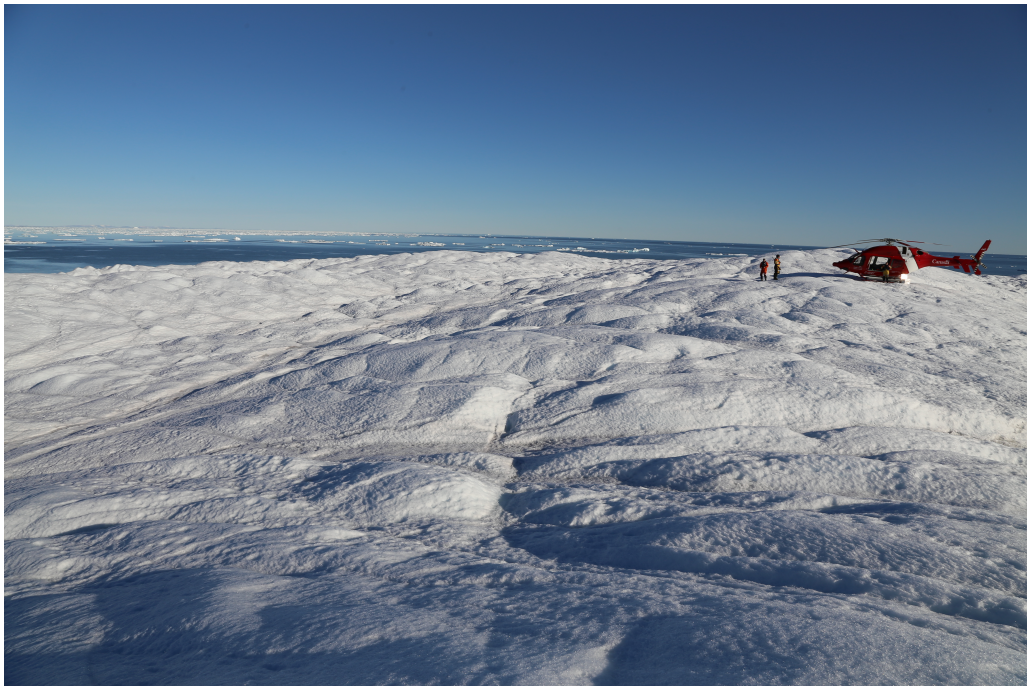

Figure 3.3: Image taken from the top of the iceberg labelled *S Nares Strait* on the day the GPS beacon was deployed. Image courtesy: Luke Copeland UO.

3.2 The RIOPS Current Data Set

The RIOPS data set has been produced as a part of the Global Ocean Data Assimilation Experiment (GODAE), an international collaboration project initiated to provide global and regional ocean forecasting systems (GODAE, 2010).

The RIOPS data set was utilized to account for the water velocity due to currents not caused by the diurnal tides. After some attempts to download the data to a local repository, it turned out to be more practical to access the data directly from the server whenever running a prediction. This saves disk space, and time spent downloading and formatting large files. The model still runs quite fast (30-45 seconds for a 48 hour prediction) even when accessing the online source. It does make the model dependent on internet access to be operational, but this can easily be worked around by downloading the data of interest.

The data was accessible in the netCDF-format, which was convenient as the OpenDrift framework includes netCDF-readers. It was, however, some issues adapt the readers to accept the polar stereographic projection used in the RIOPS data. With some help from the developers this problem was solved, future versions of the OpenDrift framework will include a feature to read such

projections. It was also necessary to modify the readers to expect the variable names corresponding with the RIOPS-data.

The data of interest contained in the RIOPS data set were the u- and v-components of the current velocity. The spatial resolution of the RIOPS is in the range of 4-5 km, with data for 50 different depths at each point (Dupont et al., 2002). The step size in depth is increasing as we go deeper. There are 13 steps for the first 21 meters and within the next 10 steps the depth is 109 meters. The deepest level included is 5875 meters.

3.3 The ERA5 Wind Data Set

The wind data contains forecast data for the u- and v-components of the wind velocity 10 meters above the sea surface. The spatial resolution is 31 km, and temporal resolution is 3 hours (Hersbach and Dee, 2016). The data was provided in GRIB-files containing data for one calendar month. Each velocity component had to be downloaded in separate files. Conversion to netCDF-format, necessary to fit the OpenBerg module, was done in a Linux environment using Climate Data Operators (CDO)-utilities. The files were concatenated into a single file containing both velocity components using netCDF Operators (NCO) in a Linux environment.

Literature on the uncertainty in ERA5 was hard to acquire. However, a report by Dee et al. (2011) was available on the predecessor to the ERA5 system, the European Reanalysis-Interim (ERA-Interim) data assimilation system. In this report, the RMSE of the wind forecasts made by ERA-Interim was in the range from [3.7, 4.0] m/s for short term forecasts. In the analysis presented in this thesis, we assume that the uncertainty in the ERA5 system is as good, or better.

3.4 The WebTide Tidal Current Data Set

It is common in most locations that *the principal lunar semi-diurnal* tidal component, also known as the M_2 tidal component, is the largest tidal constituent. Harmonic analyses of the tidal constituents in the Baffin Bay are mostly semi-diurnal in character (Greisman et al., 1986).

Tidal forcing data due to the M_2 component was acquired from the WebTide Arctic Data, issued by the Bedford Institute of Oceanography. This model uses sea surface height assimilation and bathymetry to estimate the tidal currents

and heights. WebTide is issued with a graphical user interface (GUI) including a function called WebTrack, which allows tidal current data to be generated along entire tracks for the correct times.

WebTide is limited to only provide tidal currents at a fixed depth of 50 meters. The model has however been validated using tidal component estimation techniques, and the M2 current component produced by WebTide was found to be accurate to within a few cm per second (Dunphy et al., 2005, p. 19).

4

Methodology

The goal of this thesis is to analyse the performance of the module OpenBerg, operating within the the software framework OpenDrift, for iceberg drift forecasting. OpenBerg is constructed with an aim to compare the performance of a trajectory model using a statistical approach with a trajectory model using a deterministic approach. The performance of the models will be reviewed for forecasts of up to 48 hours.

In this chapter we will discuss the two different models implemented by OpenBerg. The software framework OpenDrift will be discussed. And we will also look at how OpenBerg implements the models discussed, and review some design choices of the implementation. In addition, methods of result analysis will be reviewed.

4.1 The Deterministic Model

The most intuitive way of describing the motion of an iceberg is in terms of the various forces exerted on it, and many models have been developed using the dynamic equations to predict the drift. A selection of such models has been discussed in chapter 2.

In such approaches special care is needed when dealing with the Coriolis force, and the force associated with the sea surface slope. Some models are designed

to account for these effects such that even without forcing due to wind, the iceberg moves relative to the water. This is clearly an improbable proposition, a more accurate approach would be to derive the sea surface slope from the equations of motion for the water (Garrett, 1985).

It is useful to consider an iceberg in an idealized situation, located in an unsteady current but not affected by any external forces such as wind. It appears reasonable to suggested that the iceberg will not be able to attain the maximum speed of the water current, if such a speed duration is too short to accelerate the iceberg up to maximum speed. Garrett (1985), however, believes that this interpretation is based on the misconception that the iceberg is accelerated by the water drag. And that the iceberg in such a situation is actually accelerated by the same pressure gradients which accelerate the water itself. Therefore the iceberg will respond in exactly the same way as the water these gradients displace.

Garrett (1985) does point out that the water drag becomes relevant in the presence of external forces, and a full dynamic equation such as equation 2.5 should therefore be considered. But the icebergs response to changes in wind is relatively short (a few hours), especially in relation to the typical time scale of significant changes in wind. Therefore Garrett (1985) believes it is generally adequate to neglect the rate of change of the iceberg velocity relative to the water. And in expansion also assume equilibrium between air and water drag, the Coriolis term times the relative velocity, and possibly the wave forces too.

These assumptions leaves a quasi-steady model, which still can be quite complicated, with concerns related to shape of the iceberg and values of drag coefficients. To avoid these complications it may be adequate to assume that an iceberg moves downwind relative to the water at a constant fraction of the wind speed. This fraction was discussed in section 2.3.1, and is in the OpenBerg module set to be 2%. When creating ensembles for analysis, this fraction was varied in order to find the model variance in relation to this and other parameters.

The OpenBerg module implements a deterministic model similar to the dynamic model proposed by Kubat et al. (2005). This model was developed as an integral part of an operational model to forecast the drift and deterioration of icebergs developed by the Canadian Ice Service (CIS). Motivation behind the development of this particular model was the demand for reliable iceberg drift forecast in the Grand Banks region off the coast of Canada, due to offshore developments.

In the model presented by Kubat et al. (2005), the iceberg drift is modelled

by considering the various forces acting upon the iceberg and solving the linear momentum equation 2.5. The basic momentum equation used in this model is defined in section 2.3 in equation 2.5. The model is built upon a collection of models addressing dynamic drift of icebergs such as EI-Tahan et al. (1983), Banke and Smith (1984), Murphy and Anderson (1985), and Bigg et al. (1997).

Kubat et al. (2005) does, however, also incorporate new features such as a more detailed environmental forcing input. Notably water drag forces are calculated using current values for every 10 meter vertical interval. This calls for a more detailed description of the icebergs keel geometry.

OpenBerg utilizes a deterministic reference implementation in order to avoid the need to provide drag coefficients for wind and current. This deterministic approach does not use a force balance equation. Wind and tidal effects are modelled as additive components of drift. The drift due to winds is a fixed fraction of the wind speed set to the value discussed above (2%). The iceberg drift due to tides is modelled as equal to the velocity of the tidal current.

OpenBerg accounts for the drift due to current as a weighted average of the current vector at different depths across the draft of the iceberg. The weighting is based upon the cross-sectional area of each depth slice, calculated according to the method of Barker et al. (2004).

The overall drift is the sum of wind, tidal and current drift components.

4.2 The Statistical Model

The statistical approach to modelling iceberg drift in the OpenBerg module uses the first N hourly observations of a trajectory to estimate and extrapolate drift. The drift is calculated as a weighted sum of these measured velocities. The weights used in the OpenBerg module are related to the Lagrangian ACF, similar to the model presented by Garrett (1985). OpenBerg utilizes a single term prediction scheme as suggested in section 2.4, but allows the user to choose the time difference between the two observed points which is utilized to estimate the trajectory. In this one-term implementation, the extrapolation weight may be described as the slope of the predicted trajectory.

The extrapolation is implemented using a simple equation. When the N first points in the observed trajectory are used to estimate the extrapolation param-

eters this can be expressed as

$$p_n = St_n + p_N, \tag{4.1}$$

where p_n is the position at the point in time we wish to estimate, t_n is the time difference between point N and point n, and S is the slope of the projection trajectory. The slope is the parameter the first N points are used to estimate. The slope is estimated using the expression

$$S = \frac{D}{\Delta t}, \tag{4.2}$$

where D is the distance between the first observation and observation in point N, and Δt is the time difference between the same points.

Figure 4.1 includes two simple sketches to illustrate how the single term prediction extrapolates drift into the future, based on equation 4.1 and 4.2. The difference between figure 4.1a and 4.1b show how the choice of the parameter N effects the prediction. A longer time interval between points makes the prediction less prone to errors due to small scale oscillations in the trajectory.

Garrett (1985) cites the search for oil and gas in some offshore regions of Eastern Canada as the motivation for the developing his model. The statistical approach was used due to experiences with unpredictable low frequency currents in the ocean. Data analysis performed by Garrett et al. (1985a) lead to the conclusion that such low frequency currents tend to decorrelate over rather short scales in time and space. Therefore prediction schemes for these currents based on measurements, even quite close to a location of interest, are not reliable. Deterministic models are sensitive to error in the input data, and a method to avoid the problems related to unpredictable currents was needed.

Numerical prediction schemes for ocean currents based on the deterministic approach has also been proposed (e.g. Robinson et al., 1984). However, such a model would have to rely upon extensive input of initial values, as well as being computationally very heavy.

A modified implementation of the statistical approach can easily be designed such that the more predictable forcing components, such as wind or tides, are accounted for using dynamic modelling. In OpenBerg this is accomplished by simply subtracting the estimated drift components, due to wind and tides from the dynamic model, before calculating the weights. Then the projection of

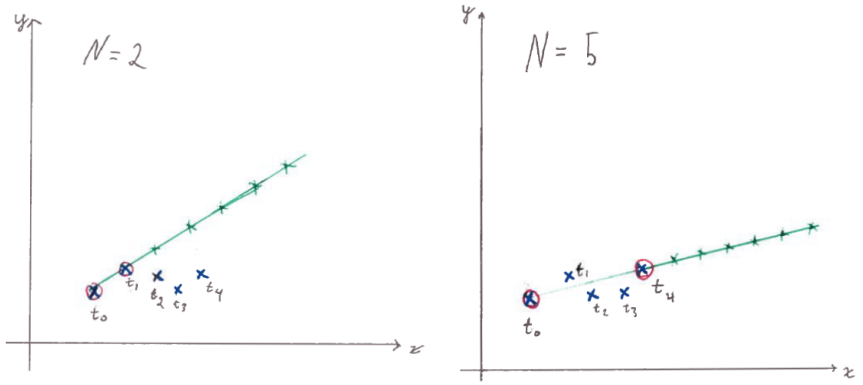

(a) (b)

Figure 4.1: In both sketches the points marked t_0, t_1, t_2, t_3 and t_4 are observed positions. The points marked with a red circle, are those used to estimate the slope (speed and direction) of the green prediction trajectory. Time steps are marked, on the predicted track, at the same frequency they occur in the observations. The spacing between these steps are determined by the estimated slope. Figure(a) show a sketch of an extrapolated trajectory with N=2, which means that the first two observations is used to estimate the slope parameter. Figure(b) show a similar sketch of an extrapolated trajectory, where the first five observations is used to estimate the slope parameter (N=5).

the trajectory, due to the residual forcing, is extrapolated using the statistical method. In the end we can add the component trajectories to find the output forecast.

4.3 OpenDrift

OpenDrift is an open source Python framework, developed by Knut-Frode Dagestad at the *Norwegian Meteorological Institute*. It was created for ocean trajectory modelling which could be used for a variety of applications, such as oil spill modelling, search-and-rescue simulations ect. OpenDrift is modular, and supports simulation of transport of any kind of particles e.g. icebergs (Dagestad et al., 2017).

It was constructed to be a framework for Lagrangian particle modelling. It is designed for flexibility, and made easy for researchers to adapt and write modules for their specific purpose.

OpenDrift uses *offline* trajectory computation, meaning that the trajectories are

computed after completion of the Eulerian simulation(s). Contrary to *online* computation, where the trajectory is computed along with the velocity fields as a part of the circulation model. This is advantageous because, for many cases, the trajectories depend on forcing from several different Eulerian models (e.g. wind, waves and currents). Offline models are also advantageous when testing modifications to the algorithms, because the full Eulerian model does not have to be rerun every time (Dagestad et al., 2017).

Most trajectory models are tied to specific applications, such as oil drift or iceberg drift, and may not be applied to other applications without compromising quality or flexibility. Many models are also impractical in that they require specific file formats, which is time consuming and effort demanding. OpenDrift has been developed with the aim to solve these and other general issues with trajectory models. It has been designed to create a framework that is able to perform all tasks commonly required for trajectory models, both oceanic and atmospheric. A central task is to obtain forcing data from various sources, and use this data to model the trajectory of the elements in space, and potentially also transform other element properties (such as evaporation of oil or degradation of an iceberg).

The OpenDrift framework is constructed with a core library aiming to extract anything common to all trajectory models of various substances and objects in the ocean and atmosphere. Several specific modules, which are ready-to-use trajectory models, are bundled into the OpenDrift code repository. It also includes a clean and generic user interface allowing for selection of module, a corresponding object or medium type, and a location and time for seeding of the object elements (Dagestad et al., 2017).

OpenDrift includes interfaces, called *readers*, suited for the most common formats of forcing data. This allows, if necessary, different modules to be forced by data from combinations of files and other sources. Readers have also been modularised, which allows any developer to create an interface towards any specific source of forcing data suitable for their needs.

After adding the readers of input data, but before running the Eulerian simulation(s), elements need to be seeded. This process accesses all data around a given number of positions and returns arrays with the values of interest. The flow chart in figure 4.2 gives a good description of how the OpenDrift framework operates. The output from this process includes the trajectory predictions due to all input components. OpenDrift provides the option to store this result in netCDF-format.

The separation of the OpenDrift core functionalities and the various modules, provides flexibility for users as existing modules are easy to modify, and new

ones are easy to create from scratch. OpenBerg, utilized for this thesis, is one such module.

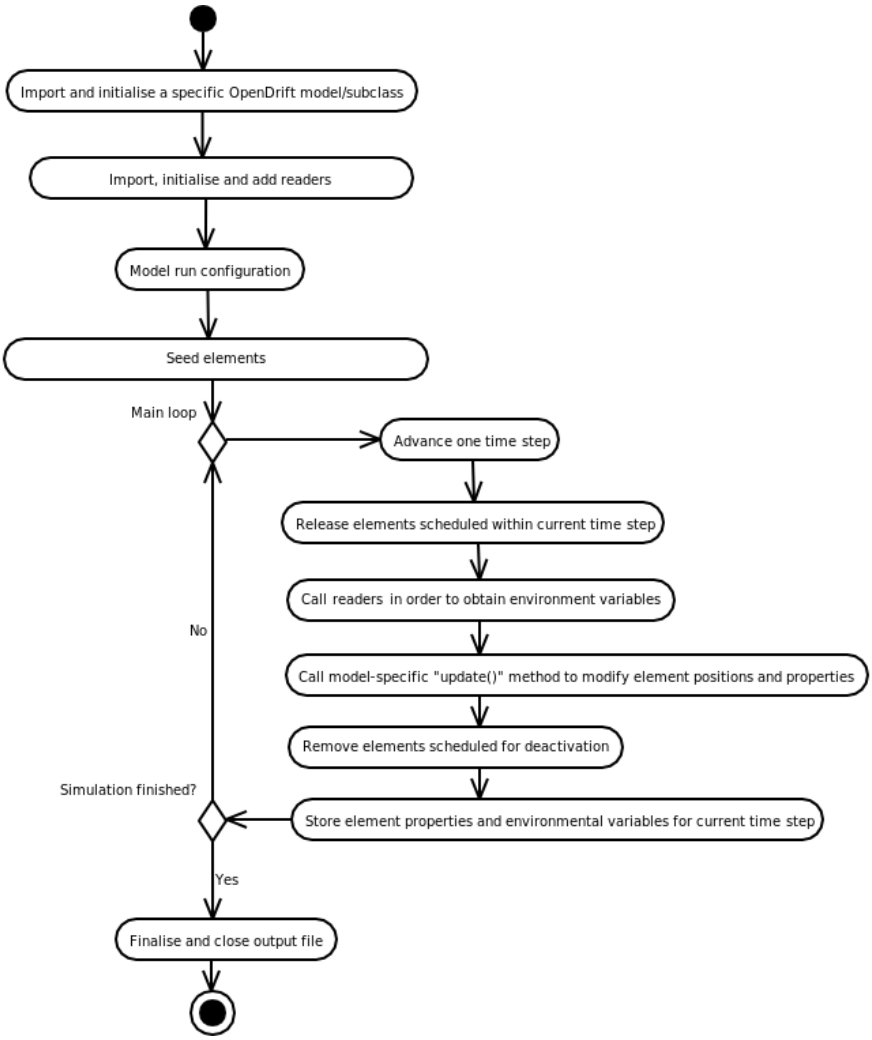

Figure 4.2: Flowchart of an OpenDrift simulation (Dagestad et al., 2017).

4.4 OpenBerg

OpenBerg is a Python software model, developed by Ron Saper at the *Water and Ice Research Laboratory* (WIRL), Carleston University, intended for comparing iceberg drift forecasting approaches. It is created as a module under the OpenDrift framework with the initial purpose to produce results comparing statistical and deterministic iceberg drift models. The work of Christopher Garrett was used as reference baseline for the implementation of the statistical

iceberg drift model (Garrett, 1985; Garrett et al., 1985a,b; Garrett, 1984). And a deterministic model based on the dynamic model presented by Kubat et al. (2005) is used.

OpenBerg is purpose-built scientific software developed to support one particular line of research. OpenBerg is still in the development stage and does not yet support any user interface. OpenBerg currently only runs using scripts, and it is necessary to edit Python code in order to control which tracks are processed, edit default parameters ect. By the developers own admission, the module is currently not suitable for real time forecast (Saper, 2017).

As the program operates under the OpenDrift framework it utilizes the included reader modules for the interpretation of the various data sets. OpenBerg does not require any other data than an observed trajectory to run. However, if the deterministic model is to be able to make predictions, it has to be provided readers with input data containing forcing fields for the track. The pure statistical model is able to make predictions only based on observational data of the iceberg motions.

A great advantage in the OpenBerg module is the ease with which one can choose prediction scheme. The default scheme when running the model is the Garrett inspired statistical-plus model. To run the deterministic model it is only necessary to enter an additional system argument string when running the script from the command window. The deterministic scheme runs when either "det" or "Det" is entered as the system argument.

The greatest advantage the OpenBerg module provides, however, is the speed at which it makes a prediction. A complete run of the deterministic model for, a 48 hour trajectory prediction, is finished in about 30 seconds. The statistical-plus model, which does not need to process as much input data, finish the same run in 5-10 seconds.

OpenBerg is equipped with a plotting function to display the observed track, the prediction track, and any component tracks used to create the prediction. These component tracks may be due to a single forcing source or the extrapolated component. This function is designed to make it easy to choose which of these tracks to include in the plot, before initializing the model. It allows the option to display any number of these tracks in the same figure.

4.4.1 Statistical-plus and Deterministic Forecast

The OpenBerg module utilizes the OpenDrift framework to run the Eulerian simulations. These simulations operate according to the flow chart in figure

4.2. The OpenBerg-module is the subclass defining the calculations that are specific to an iceberg, discussed in this chapter and in section 2.2.

The input needed for these simulations are the vector fields of the various forcing components driving the drift, and a file containing the coordinates of observed iceberg track. The OpenBerg module expects files containing the velocity fields of the following forcing components:

- Currents
- Tides
- Winds

The user also needs to define a map-projection that the trajectory predictions are projected on to. Functions to create the map are provided with OpenDrift. The output from the Eulerian simulations are the tracks, due to the various forcing fields, guiding the iceberg drift. Alongside the simulations, the observational data is converted to the same projection as the trajectory components in the output.

The outputs from the Eulerian simulations are utilized differently in the statistical-plus and deterministic models. In the deterministic model the output trajectories from this model are simply added together to form the final prediction trajectory. The statistical-plus forecast uses the statistical modelling principles to replace the drift component due to currents, while still including the drift components due to wind and tides from the Eulerian simulations. This scheme uses these outputs from the Eulerian simulations and subtracts the contributions of wind and tidal effects from the observation data. Next it uses the first N hourly samples to estimate and extrapolate the residual component. Finally the wind, tide and extrapolated components are added back together to form the final statistical-plus prediction trajectory.

To illustrate the processing of the outputs from the Eulerian simulations in a more comprehensible fashion, figure 4.3 show different steps of the process. Each figure includes the same observed track but the other tracks included differ. In figure 4.3a the deterministic components due to *wind only* and *M2 tide only* are plotted, along with the *residual* track. The residual is the remaining component, after subtracting the wind and tide tracks from the observed trajectory. The model uses the first N time steps in the residual track to extrapolate a prediction for this component. The residual trajectory is replaced in figure 4.3b by the *extrapolation* component. Then the sum of all components in figure 4.3b is added together and plotted as the statistical-plus prediction in figure 4.3c. Due to the first N time steps being used to extrapolate,

we can see in the plot that the prediction does not start until step N. Figure 4.3d shows the deterministic prediction for the same trajectory, with all components and the final prediction plotted together.

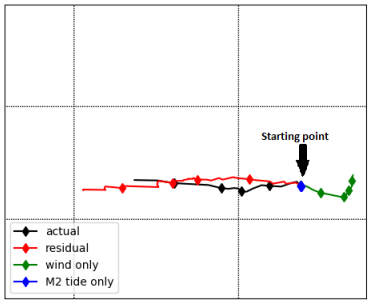

(a) Residual component.

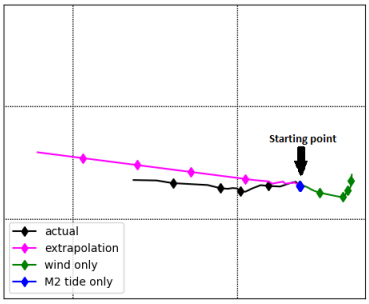

(b) Extrapolated residual component.

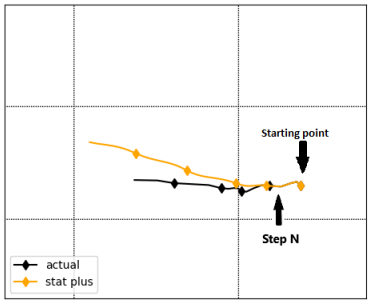

(c) Statistical-plus prediction.

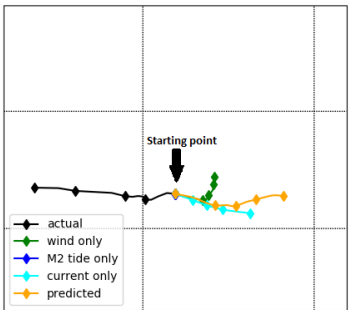

(d) Deterministic prediction.

Figure 4.3: Figure(a) shows a plot of the modelled trajectory components due to *wind only* and *M2 tide only*, along with the observed trajectory, labelled *actual*, and the *residual* component. The residual component is the result from subtracting the wind and tide components from the observed trajectory. Figure (b) shows the same trajectories as in (a), but the residual has been replaced by an extrapolated component, labelled *extrapolation*. The first N steps in the residual from (a) is used to extrapolate the component in (b), therefore the first N steps in these components are equal in (a) and (b). Figure (c) shows the statistical-plus forecast together with the actual track. In this plot the *stat-plus* component is equal to the sum of the wind, tide and extrapolated components. Figure (d) shows the corresponding forecast using the deterministic model. All components are the same, but the extrapolated component is replaced by the *current only* component. The predicted trajectory, labelled *predicted*, is the sum of wind, tide and current components.

In the current version of OpenBerg, only the observed trajectory is required as input. It is possible to run the model with input data for just one or two, or even none of the forcing fields. In this case, the model will assign the default value of zero to the entire missing forcing field. As a result, the plus-function will be turned off and the model prediction will be purely statistical.Hence, the trajectory forecast is created by extrapolating the entire track. The deterministic

model, on the other hand, will not be able to make any predictions without any input forcing fields provided.

4.4.2 Updates by the Author

For the purpose of this thesis, some updates were necessary to customize the module to the data. Some changes were made to make the module faster and more practical for certain applications. For the purpose of the result analysis, presented in chapter 5, it has also been added a few new functions to the OpenBerg module. The following updates was made:

- The software is at the moment still of limited flexibility when it comes to input formats. The readers provided with the OpenDrift framework expected different variable names to those in the data sets used for this thesis. To adapt the module to the format, some modifications of the OpenDrift readers, utilized by OpenBerg, were required. The problem was solved by changing the name expected by the readers.

- It was necessary to hard code an addition into the netCDF-reader module for it to correctly interpret the map projection used in the files containing the forcing data for currents. This data was stored on a polar stereographic projection. Originally OpenBerg was only able to read a longitude/latitude-grid projection.

- The version of OpenBerg, made available for this thesis, required that forcing data due to currents was provided. This requirement was removed because this data is not utilized in the statistical-plus prediction, and including it slowed down the run time considerably. In addition, this dependency is impractical if such data is unavailable and one only wishes to use the statistical-plus model.

- The prediction scheme was updated to include an option to adjust the strength and direction of the trajectory components due to both currents and winds. This was done to be able to perform an ensemble analysis. The adjustments were made using simple geometry, explained in more detail in section 4.4.3.

- A new function which calculates and plots the deviation of the prediction from the observed path, was added to the OpenBerg module. This function can also be utilized to store these values in text files for further analysis. To calculate the distance between the two tracks at each point the function uses the *Haversine*-formula. This formula calculates the distance between two points on the surface of the Earth, using the

longitude/latitude coordinates. A rendering of the Haversine formula is showed in equations 4.3 through 4.6 (Rick, 1999):

$$\begin{aligned} dlon &= lon_2 - lon_1, \\ dlat &= lat_2 - lat_1, \end{aligned} \tag{4.3}$$

$$a = \left(sin\left(\frac{dlat}{2}\right)\right)^2 + cos(lat_1) \cdot cos(lat_2) \cdot \left(sin\left(\frac{dlon}{2}\right)\right)^2, \tag{4.4}$$

$$c = 2 \cdot arctan\left(\frac{\sqrt{a}}{\sqrt{(1-a)}}\right), \tag{4.5}$$

$$d = R \cdot c, \tag{4.6}$$

where d is the distance between points $p_1 = (lon_1, lat_1)$ and $p_2 = (lon_2, lat_2)$, and R is the radius of the Earth.

- Another function was built to plot the position of a single point of the actual track relative to the position of the same point in the prediction. This function is utilized to comment on the presence of a systemic error in the model.

4.4.3 Analysis

To assess the performance of the model the original intention was to perform an ensemble analysis of both the deterministic model and the statistical-plus model. The aim was to determine the distribution of the predictions based on the sensitivity to parameters and input forcing fields. However, the results from the deterministic model proved to be so poor that this plan was changed and the ensemble analysis was only preformed on the statistical-plus model.

The analysis of the deterministic model was reduced to a study of the sensitivity to the size parameter. The reasons for choosing this method and the results from the analysis is further discussed in chapter 5.

Ensemble analysis is utilized to determine the distribution parameters for the predictions made by a model. Before the analysis can be performed, a reasonable range must be determined within which the forcing fields (or parameters)

are allowed to operate. Then an ensemble of predictions is produced where these forcing fields are allowed to operate within the chosen range.

When an ensemble has been created, the distribution of the predictions can be evaluated, and ensemble parameters can be estimated. Important parameters to estimate is the variance and the SD. The mean error in the ensemble can also be estimated. However, in the analysis this thesis performs, it makes more sense that the error in the original prediction trajectory is assumed to be the mean (as this is the basis for the ensemble).

To analyse the OpenBerg module, a small section of one of the tracks from the Baffin Bay data set was chosen for testing. The same track section was used to analyse both the deterministic and the statistical-plus model. To evaluate the effect of uncertainty in the wind data, the direction and power of this forcing component was manipulated to create ensembles. Different ensembles were created for different values of N (the number of observations used to extrapolate the residual component). A random number generator was used to produce adjustment angles in a given range. The same generator was used to produce factors (in a different range) which adjusted the strength of the forcing field.

The method used to adjust the trajectories is based on simple geometry. Each point in a trajectory can be described by a position vector relative to the starting point of the trajectory, $\mathbf{r} = (x, y)$. After adjusting the trajectories each new position vector is described by a new set of coordinates, $\hat{\mathbf{r}} = (\hat{x}, \hat{y})$. For each position vector in a trajectory, the magnitude was calculated using Pythagoras theorem

$$|\mathbf{r}| = \sqrt{x^2 + y^2}. \tag{4.7}$$

The angle of the vector θ, was calculated

$$\theta = arctan(\frac{y}{x}). \tag{4.8}$$

Then the magnitude was adjusted by a factor p, provided by the random number generator

$$|\hat{\mathbf{r}}| = p|\mathbf{r}|, \tag{4.9}$$

where $\hat{\mathbf{r}}$ denotes the adjusted vector. The angle was adjusted by an adjustment angle $\Delta\theta$, provided by the random number generator

$$\hat{\theta} = \theta + \Delta\theta \tag{4.10}$$

where $\hat{\theta}$ denotes the adjusted angle. Finally, the new vector coordinates are calculated

$$\begin{aligned} \hat{x} &= |\hat{\mathbf{r}}|cos(\hat{\theta}) \\ \hat{y} &= |\hat{\mathbf{r}}|sin(\hat{\theta}) \end{aligned} \tag{4.11}$$

Figure 4.4a shows a sketch of the adjusted position vector looks relative to the original vector for a single point. In figure 4.4b an example is plotted showing how an entire trajectory looks after adjustment, relative to the original track.

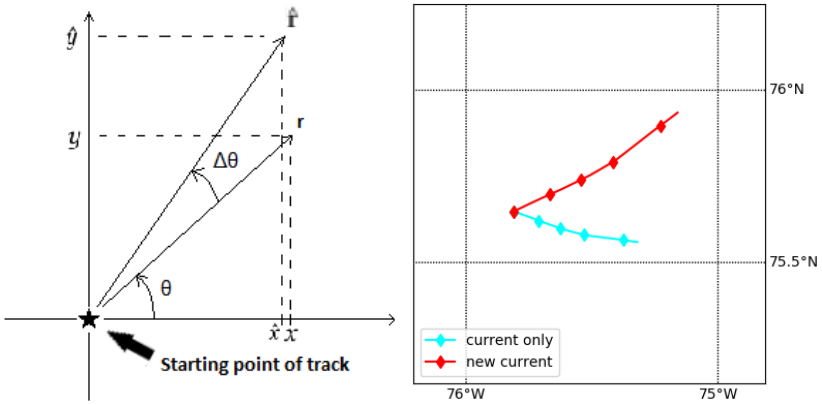

(a) **(b)**

Figure 4.4: (a) is a sketch of a single position vector before and after it is adjusted according to equations 4.7 through 4.11. (b) displays an example plot of how an entire trajectory looks, relative to the original track, after adjusting the coordinates in all points. The track labelled *current only* is the original, and the one labelled *new current* is the adjusted track. The value of the parameters used is $p = 1.5$ and $\Delta\theta = 45°$.

5

Results and Discussion

This chapter will include results and discuss the performance of the OpenBerg module. Predictions using the pure statistical scheme, the deterministic scheme, and the statistical-plus scheme will be presented.

The discussions regarding the statistical model will be limited and does not include an extensive performance analysis. These results are included in order to show the reader how this component of the model works, and show the results from this scheme. The results and discussions about the prediction capabilities of the deterministic and statistical-plus schemes are discussed more thoroughly. The analysis is performed based on a sensitivity study on the deterministic model and an ensemble analysis on the statistical-plus model.

5.1 A Consideration of Track Selection and Choice of Analysis Method

All the tracks from the Baffin Bay data set are plotted in figure 3.1. As evident from the plot, the length of each path varies considerably. Some of the tracks appeared to be grounded for extended periods and were therefore useless for testing of the OpenBerg model. There were, however, extended periods available for several tracks. A small section of the track labelled *SNaresStrait* was selected for the main part of the analysis.

The SNaresStrait track is plotted in figure 5.1. The movements of this particular iceberg were recorded from August 17 2016 until December 12 of the same year. The following analysis aims to assess the short term prediction capability of OpenBerg. Therefore only a 48 hour window from this track is selected for analysis, from 2016-09-21 at 15:00 to 2016-09-23 15:00.

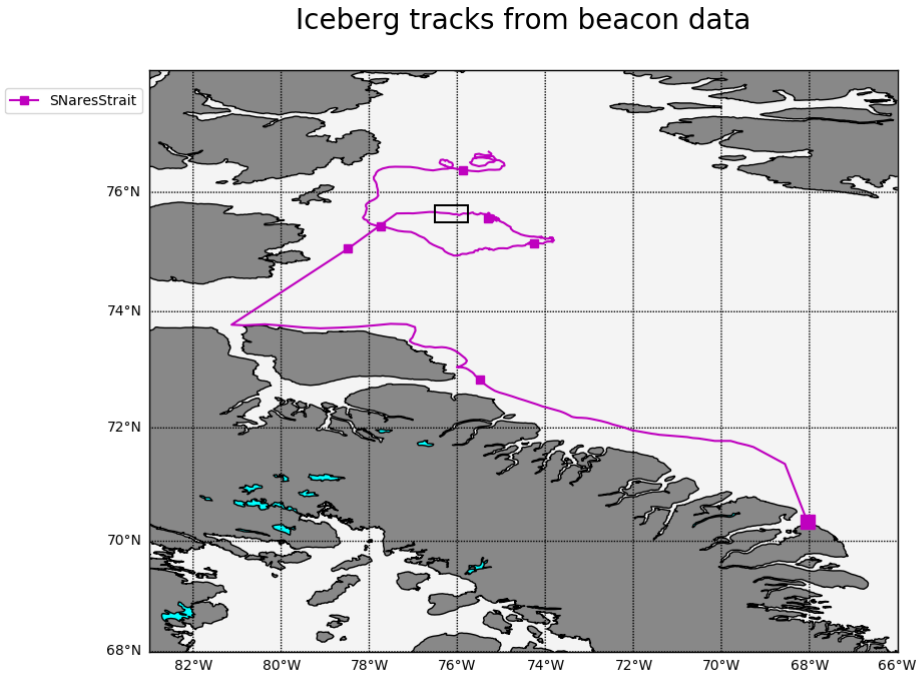

Figure 5.1: Plot of the observed track of the iceberg labelled SNaresStrait, from the Baffin Bay data set. The end point of the track is represented by a larger marker. The section of the track used for analysis is marked with a black box.

The initial intention was to adjust forcing due to wind and currents in order to create ensembles to analyse the performance of the deterministic model. However, the accuracy of the prediction output from this model turned out to be so poor that there was no value in such an analysis. Therefore the performance analysis of the deterministic model was limited to a sensitivity study of the parameter describing the size of the iceberg. The reasoning behind limiting the analysis is further discussed in the following sections.

The results from the statistical-plus model provided a more accurate prediction relative to the observed GPS-track, compared to the deterministic model. Ensembles were created for this model by adjusting the power and the direction of the wind component. Three ensembles were created using different number of

observations, N, for extrapolation of the residual component. The tidal component was not analysed using ensembles due to the well documented accuracy of the prediction systems of this component (Greisman et al., 1986). In addition to the expected accuracy of the tide component, its contribution to the projected drift is relatively small compared to the other forcing components.

To be able to compare the prediction from the two models, the prediction has to start at the same point. The statistical-plus model uses N hourly observations preceding 15:00 2016-09-21 to extrapolate the predicted track. Therefore these N-1 extra steps are included in the output trajectory plots from the statistical and statistical-plus prediction schemes. If N=2 one extra point is included, if N=10 nine extra points is included in the plot. Note that in figures displaying outputs from the statistical and statistical-plus models, the prediction trajectory is equal to the observed track for the first N steps in the plots. However, every output displayed starts the prediction into the future at the same point in time and predicts a 48 hour track. This mean that the time at the endpoint in all plots is 2016-09-23 15:00.

5.2 The Statistical Model

In this section some results from testing the pure statistical model is presented. The intention is to show how the techniques described in sections 2.3 and 4.2 performs in the version implemented in OpenBerg. No extensive analysis of this model is attempted, as it is not able to account for variable forcing conditions.

5.2.1 Prediction Output

The statistical predictions are made by running the statistical-plus model without input forcing fields. Without forcing data provided as input to the statistical-plus model, the extrapolated component is equal to the (entire) prediction. The plots of the output from the statistical predictions includes these two tracks labelled *extrapolation* and *stat plus*. Both these tracks are included in order to make the plots more comparable to the statistical-plus plots presented in upcoming sections. When the statistical-plus model is provided with forcing data, these two trajectories will differ from each other. In addition, the observed trajectory is also included in all plots.

In figure 5.2 we see the statistical prediction on the chosen track segment using only two points (N=2) to extrapolate into the future. It appears that in this short time span the extrapolated trajectory was able to predict the direction

of the future drift quite well, but the length of the iceberg track is not quite accurate. The error in the endpoint of this predicted track is 21.87km.

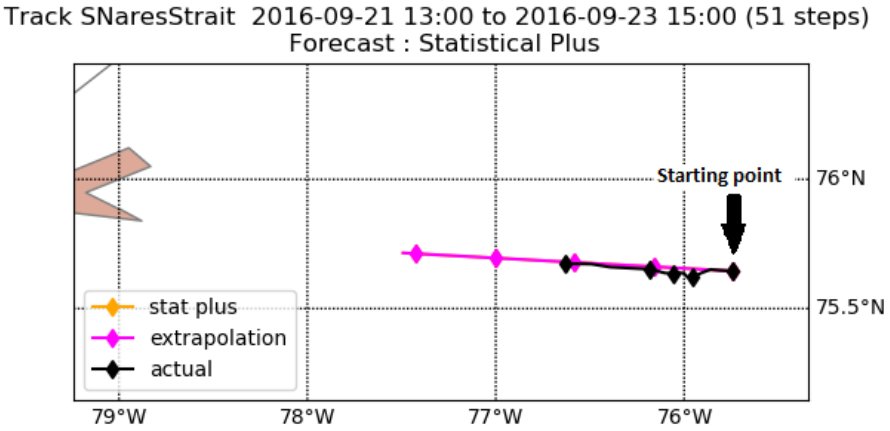

Figure 5.2: Plot of a statistical-plus prediction done without input forcing fields, for the SNaresStrait iceberg with N=2. Included (in the plot) is the observed trajectory, labelled *actual*, the drift forecast using the statistical-plus model, labelled *stat plus*, and the extrapolated track, labelled *extrapolation*. As no forcing data is provided as input the prediction is purely statistical. Therefore, the statistical-plus prediction and the extrapolated track are the same.

In figure 5.3 we see the same plot as in figure 5.2 but using six points (N=6) to extrapolate into the future. In figure 5.3 both the direction and magnitude of the predicted track is different from 5.2. The direction is not as accurate in the new prediction, but the length of the track is more precise. The error in the endpoint of the predicted track when N=6 is 15.11km.

In figure 5.3 it is also clearer to see that the start of the prediction is delayed by N points, as the prediction track and the other tracks plotted are the same for the first N points. Please note that prediction time is set such that the actual prediction starts at the same point in both these plots and all other results presented in this chapter.

In figure 5.4 we again see the track section as in figures 5.2 and 5.3, but now for a statistical prediction with N=10. Again we see a change in the direction, and

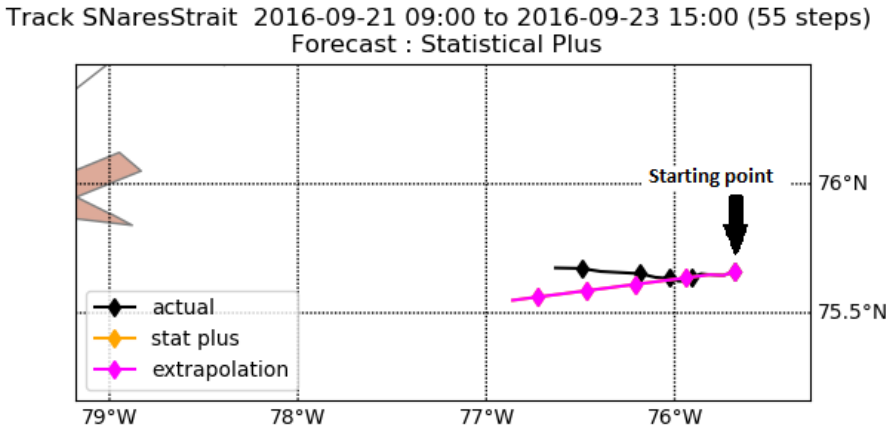

Figure 5.3: As figure 5.2, but with N=6.

a change in magnitude of the predicted track. This prediction is actually very accurate, and follow the observed track closely along the whole track. And in the end point the error is only 3.71km.

5.2.2 Discussion

The results presented in figure 5.4 looks promising, with a very accurate prediction. But the problem with the pure statistical prediction model, is that the one term prediction scheme is not able to account for oscillations that may occur in the actual trajectory (within the period used to estimate the extrapolation weight). Such a model is very sensitive to outliers in the sampled observations, and it has no ability to predict the oscillating components of the drift.

The result in figure 5.2 is quite lucky, in the sense that the direction was accurate. It could just as easily suffer from a bad sample such as in the example sketch in figure 4.1a. The distance between the first two points, used for this extrapolation, obviously did not give a good representation of the future velocity of the iceberg. This caused the error to eventually be quite significant, even with the accurate representation of the direction.

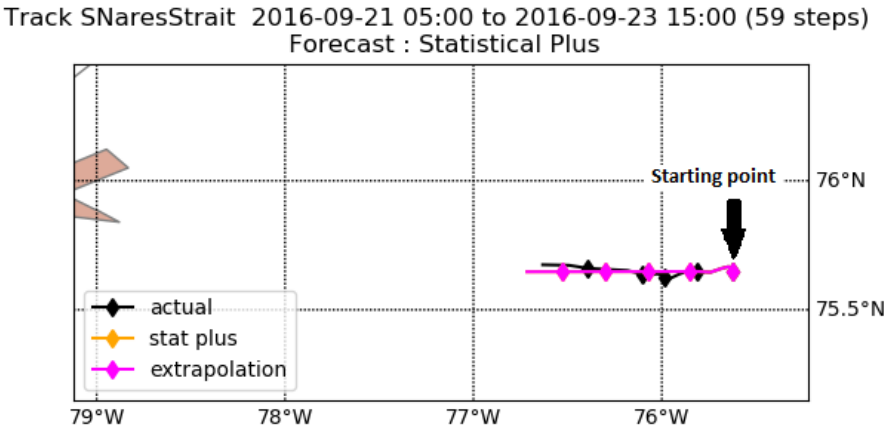

Figure 5.4: As figure 5.2 and 5.3, but with N=10.

The following two test runs presented in figures 5.3 and 5.4 show how increasing the time interval between the samples decreases the vulnerability to outliers. The error decreases when N increases. A problem with just increasing N, is that eventually the correlation between observations will be lost and the predictions will not be of any value. Also, how large N should be is not obvious and depends on what scale small oscillations in the track takes place, in both space and time. These scales will be different for different tracks, and different track sections.

A way to account for these oscillations and be able to use the statistical method on a track where the oscillations are accounted for is to introduce the statistical-plus model. By introducing some predictable forcing components, the statical part of the modelling is required to account for less variation. Thereby it should be less vulnerable to outliers in the sampling. A more detailed analysis of the statistical-plus model is discussed in section 5.4, but first an analysis of the deterministic model.

5.3 The Deterministic Model

Results from the testing of the deterministic model is presented and discussed in this section. First the output from the model applied to the chosen track section is presented and commented on, then a sensitivity study of the iceberg-size parameter is performed and discussed.

5.3.1 Prediction Output

The output from the deterministic model includes a predicted trajectory for the iceberg along with separate predicted trajectories for every forcing component.

The predicted trajectory using the deterministic model including all forcing components yields the output plotted in figure 5.5. The black trajectory in the plot, labelled *actual*, is the observed trajectory. All predicted tracks due to individual forcing components (wind, tides and currents) are also plotted, with labels *wind only*, *M2 tide only* and *current only*. The yellow trajectory labelled *predicted* is the sum of all the forcing components, and is the outputted drift forecast from the deterministic model.

Note that it is not possible to see the *M2 tide only* trajectory (the component due to tidal effects), because it is covered by the other tracks. This is because the track due to tides on its own only causes relatively small motions. The estimated trajectory due to tides only causes the iceberg to oscillate about the starting point. The tidal track is plotted together with the observed track in figure 5.6 to illustrate this. The plot display the same track component as in 5.5, just slightly zoomed in.

From visual inspection of the result plotted in figure 5.5, it is obvious that the prediction is not good as it deviates a lot from the observed track. The prediction in the end point of the trajectory is off by 39.7 km. However, the major issue is that the predicted trajectory moves in the opposite direction of the observed track. Inspecting the various component trajectories, both the current and wind trajectory components appears to be contributing to a prediction that is moving in the wrong direction.

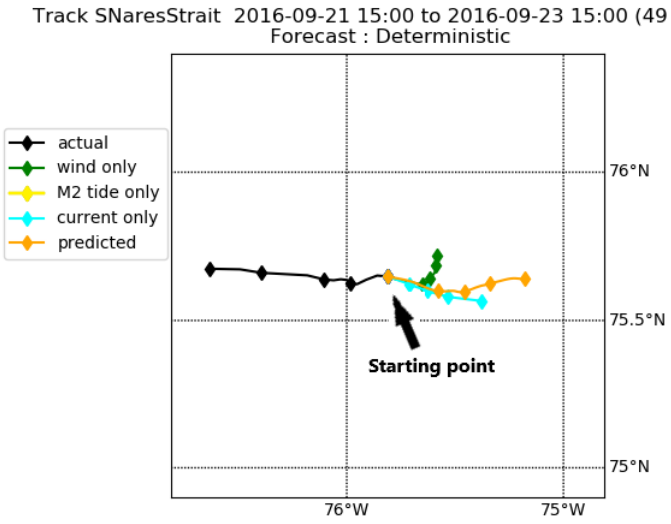

Figure 5.5: Plot of observed trajectory, labelled *actual*, along with the drift forecast using the deterministic model, for the iceberg labelled SNaresStrait. The *predicted* trajectory is the model prediction, and equals the sum of projected trajectories due to tides, winds and currents. The individual component trajectories are also included in the plot. The track labelled *current only* is the component due to the current forcing field. The track labelled *wind only* is the component due to the wind forcing field. The tidal forcing component is labelled *M2 tide only*, however, it is relatively small compared to the other trajectories plotted an is therefore not visible.

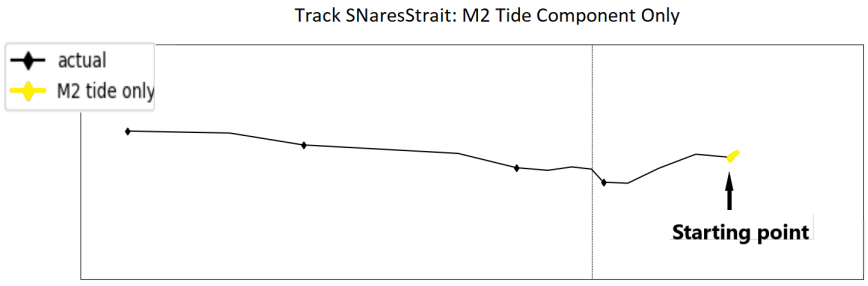

Figure 5.6: This is the same plot as in figure 5.5, but zoomed in and including only the *actual* track and the trajectory component due to *M2 tide only*.

5.3.2 A Sensitivity Study

Due to the poor initial results from the deterministic model the decision was made to perform a sensitivity study on the chosen parameter of iceberg size.

This is a parameter which should be important to the response of the drift due to current forcing, and it is interesting to see if varying the size of the iceberg changes the predicted iceberg trajectory significantly.

The OpenBerg module models composite icebergs calculating size and shapes based on equation 2.19, using the parameters listed in table 2.1. However, the current version of OpenBerg is simplified such that it only has the option to choose between four different sizes: *SM*, *MED*, *LG* and *VLG*. In table 5.1 the waterline lengths and keel depths corresponding to the different size labels are listed. This rigid implementation is practical if the model is to be applied to an iceberg where the exact measure of the waterline length is uncertain. And it makes a parameter sensitivity study even more relevant.

Table 5.1: Corresponding waterline lengths (L) and keel depths to the different size options available in the OpenBerg module. L is inserted into equation 2.19 using parameter values from table 2.1 to create composite icebergs.

Size Label	Waterline Length (L)	Keel Depth
'SM'	37.5 m	30 m
'MED'	90.5 m	60 m
'LG'	160.5 m	110 m
'VLG'	277.5 m	200 m

The same track section as displayed in figures 5.5 through 5.9 was used for the sensitivity analysis. The size class used to make the prediction trajectory in figure 5.5 was *LG*. In figure 5.7 the observed track for the same track section is plotted along with the predictions using all size classes. The difference we observe between the different predictions is noticeable, but compared to the actual error in the model it is insignificant. Clearly it not this parameter that is the main source of error in the predictions.

It could be argued, from looking at the photographs in 3.2 and 3.3 that the measurements of the *SNaresStrait*-iceberg corresponds better to size class *VLG* than to *LG*. However, changing from *LG* to *VLG* only reduces the error in the model from 39.7 km to 37.8 km. It is evident that this parameter mainly contributes to the magnitude of the current component, the error in the direction of the prediction is still just as significant.

If it is assumed that more accurate forcing data is provided this analysis would be a lot more interesting, as it clearly is a response in the predictions to this parameter.

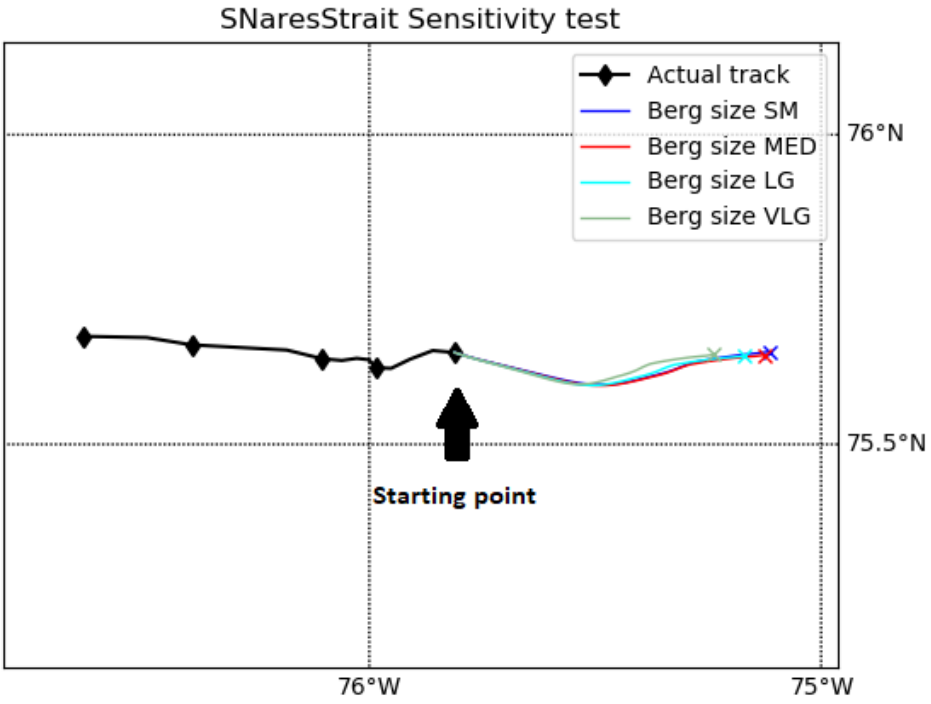

Figure 5.7: Plot of the sensitivity test to the size parameter. The black trajectory is the observed drift path, while the other tracks are the predicted trajectories for the various sizes available in the model. All forcing components are included. The only difference, between the various predicted trajectories, is that the iceberg size parameter is changed. The end point of each of the prediction tracks are marked with a ×-marker.

5.3.3 Discussion

It could be argued that the other forcing components may be significant sources of error as well, but it is very clear that the current component is not accurate. In the following section we will see that we obtain a much improved result using the statistical-plus model. The statistical-plus scheme replaces the current component from the deterministic model by an extrapolated residual component. The combination of these results points towards the current component being the principal source of error in the deterministic output. This aligns with the proposed need to develop methods which does not rely upon

current forecasts as input for iceberg trajectory forecasting, which is discussed in previous chapters.

It was of interest to see how much of an adjustment to the current component was necessary to produce a prediction close to the observation. The current component was manipulated and played with, while holding the other forcing components constant, in order to find a good prediction. Eventually, by adjusting both direction and power of the current forcing, the result in fig 5.8 was produced. The angle of the forcing was adjusted 162.5° clockwise and the length of the component increased by a factor of 2.35. The error is forced down to below 1 km in the end point of this manufactured prediction. The new prediction trajectory actually follows the observed track quite close along every step of the prediction.

Comparing the adjusted *new current* component to the original, unmanipulated, component *current only* in figure 5.8 is disconcerting. It is clear that the input forcing data for this point in time and space is not only inaccurate, but completely wrong.

Any further analysis of the deterministic model was abandoned due to the result from the initial test run and the sensitivity study. Combined with the comparison to the statistical model it was concluded that the error in the current data was to great to produce any meaningful results using the deterministic prediction scheme.

5.4 The Statistical-Plus Model

Results from the testing of the statistical-plus model is presented and discussed in this section. First the output from the model applied to the chosen track is presented and commented, then an ensemble analysis is performed where the wind forcing field is adjusted to create the ensembles. To make the results in this section comparable to the results using the statistical and deterministic schemes, the analysis in this section is of the same track section that was used in previous sections.

5.4.1 Prediction Output

The output from the statistical-plus scheme is in essence a made up of a combination of the statistical model and the deterministic model. Each predicted trajectory is made up of the same components as the deterministic output, but with the current component replaced by an extrapolated residual component.

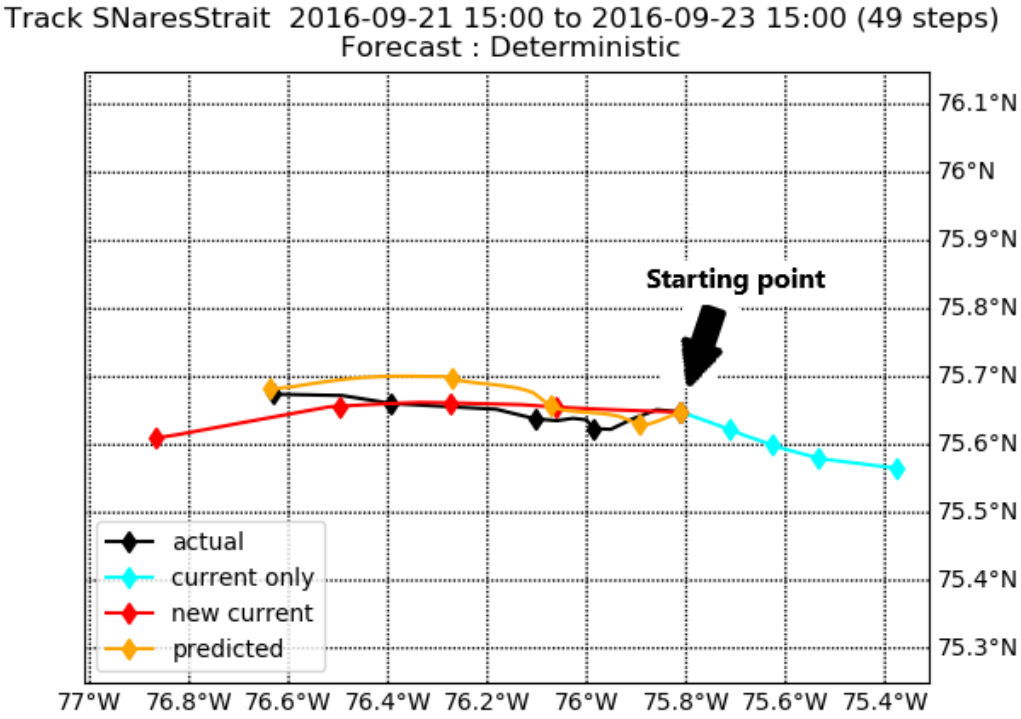

Figure 5.8: Plot of the best result produced by adjusting the current forcing. Included in the plot is the observed drift path in black, labelled *actual*, the original *current only* track in blue, and the adjusted *new current* track in red. The new current track equals the current only track with the power increased by a factor of 2.35, and the angle adjusted by 162.5°. The adjusted prediction is included as the yellow *predicted* track, it is the sum of the new current track, the *tide only* track and the *wind only* track. The tide and wind components are the same as in 5.5.

This component is estimated in the same way as in the statistical model, but after first subtracting the wind and tidal components from the observed track. The first N observations in this residual track is used to extrapolate this component into the future. If this description is unclear, a look at figure 4.3 may be helpful.

The prediction from the statistical-plus model is plotted in figure 5.9. This output was produced using the same input data as in the results presented in the previous sections. In the presented result, N=6 time steps are used to estimate the residual component. This component is plotted as the purple trajectory labelled *extrapolation* in figure 5.9. Also plotted is the model prediction labelled *stat plus*, the observed track labelled *actual*, and the wind component labelled

wind only. The tidal component is excluded from the plot because it is to small to see, but it is included in the prediction trajectory.

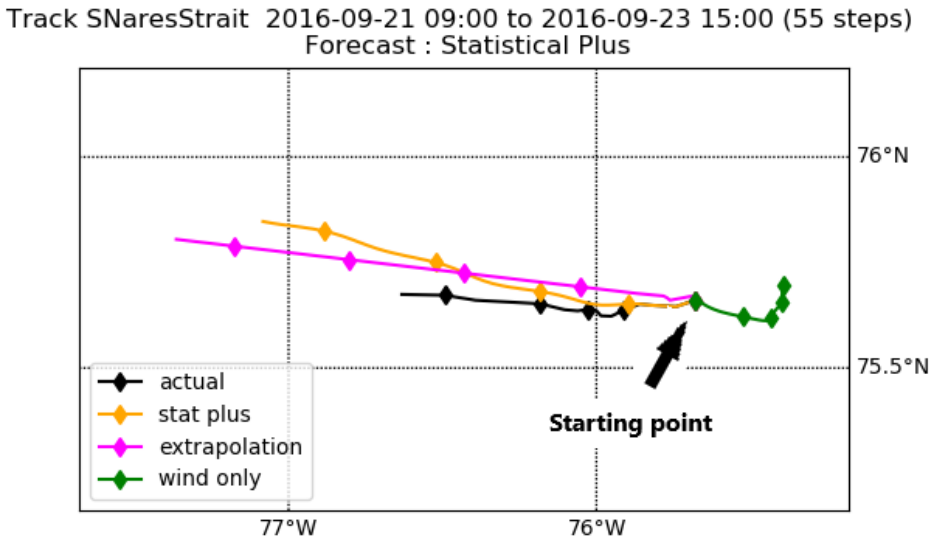

Figure 5.9: Plot of observed trajectory, labelled *actual*, along with the drift forecast for the iceberg labelled SNaresStrait. This result was produced using the statistical-plus scheme, with N=6. The track labelled *extrapolation* is the extrapolated residual component. The track labelled *wind only* is the projected component due to the wind forcing field. The *stat plus* trajectory is the model prediction, it equals the sum of projected trajectories due to tides and winds as well as the extrapolated component. The tidal forcing component (which is the same as in figure 5.5) is not displayed in this plot, but it is included in the *stat plus* trajectory.

In comparison to the deterministic forecast in figure 5.5, the prediction from the statistical-plus model in figure 5.9 appears to be much better. The direction of the predicted trajectory is significantly closer to the actual track. It is, however, still off by 22.3 km in the final step of the prediction. This error is significant considering that the iceberg only travelled 21.9 km in total, according to the GPS-data.

The deviation curves for the predictions in figures 5.9 and 5.5 are plotted in figure 5.10. We can read from those plots that the deviation is smaller for more or less every time step in the statistical-plus prediction, compared to the deterministic prediction.

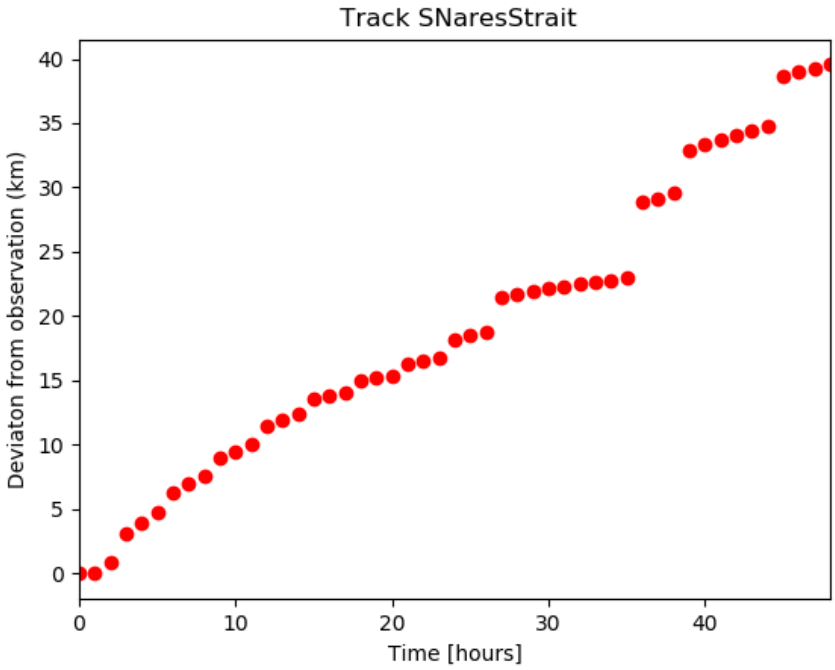

(a) Deterministic

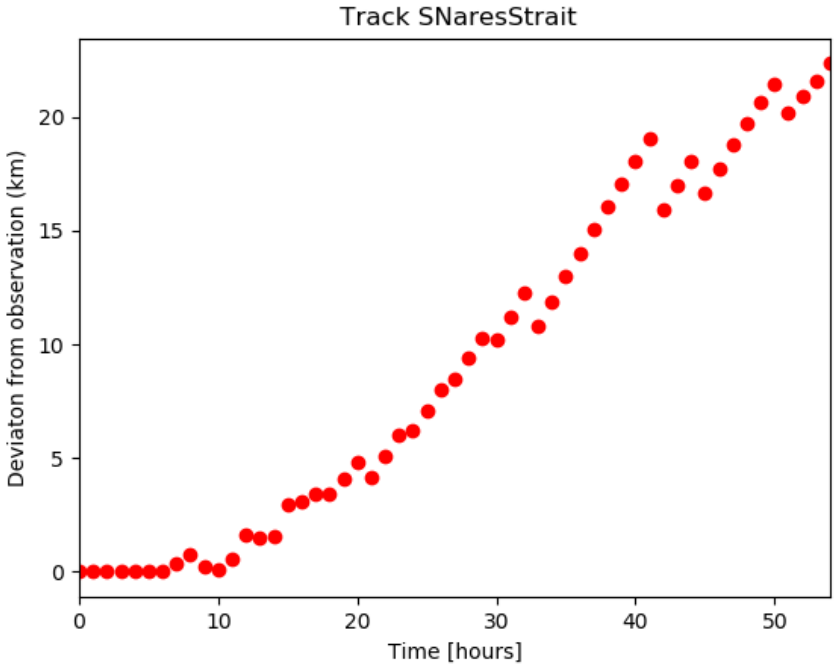

(b) Statisical-plus

Figure 5.10: Distance from the prediction to the observation. (a) is the plot for the deterministic prediction displayed in 5.5, and (b) is the plot for the statistical-plus prediction displayed in figure 5.9. The x-axis is the time passed in hours, and the y-axis is the distance from the observed position to the predicted position at the corresponding time. Note that the N=6 points used for extrapolation is included in figure (b).

5.4.2 Ensemble Analysis

In order to analyse the performance of the statistical-plus model, an ensemble analysis was performed. The aim was to determine the distribution of the predictions based on the sensitivity to parameters and input forcing fields.

The most important parameter choice in the statistical-plus scheme is the fraction of the wind speed at which the iceberg moves. There is also some uncertainty related to the accuracy of both the direction and power in the wind forcing data set. As mentioned above, the forcing due to tides was not analysed using ensembles. This was due to their relatively small contribution to the drift prediction, and the accuracy of existing tide models.

The wind speed fraction is the fraction of the wind speed at which the iceberg is displaced. The default value of this parameter in the OpenBerg module is 0.02, chosen based on previous studies and other models (e.g. Smith, 1993; Bigg et al., 1997). Inaccuracies in the magnitude of the predicted wind component could be caused by this wind fraction parameter being wrong. However, it might also be caused by errors in the forcing field of the wind data. It is difficult to determine which of these is the main source of any uncertainty and no attempt has been made to separate them. And the parameter and forcing field are evaluated as one common source of uncertainty in the ensemble analysis. The direction of the forcing field in the wind data may also be a source of error, and is included in the analysis.

To account for all the possible uncertainties in the drift forecast, related to the wind forcing, the wind trajectory was adjusted to create ensembles. The ranges of the parameters used to adjust the wind trajectory was chosen based on the prior knowledge about the uncertainty in the data set, discussed in section 3.3. The magnitude of the wind vectors in the ERA5 data set, along the track used for analysis, was in the range [3.0,9.0] m/s. With the RMSE reported by Dee et al. (2011) ($\sim$ 4.0 m/s), we get a range with uncertainty: [3.0 $\pm$ 4,9.0 $\pm$ 4] m/s.

The power of the wind forcing was adjusted by multiplying the length of the position vector (relative to the starting point) at each point in the wind track by a power factor. The power factor was defined to be in the range [0.25,2], which based on the prior knowledge was considered to account for the wind speed uncertainty in the ERA5 data set. These factors were produced by a random number generator producing numbers from a uniform distribution in the given range.

No literature was found on the accuracy in the direction of the wind forecasts. Therefore, to be sure that the ensemble accounted for the uncertainty in

the direction of the wind, a wide range was used for this parameter in the ensemble. The trajectory was adjusted by angles in the range [-45°,45°]. The same uniform number generator that was used to produce the power factor was used to provide the the angle values (but in the different range).

Note that for each time the wind is adjusted, a new residual track is estimated. This mean that a change in wind forcing causes a corresponding change in the extrapolated component. The results show that the effect on the prediction reducing the magnitude of the wind component, was a shortening of the projected iceberg track. Figure 5.11 shows a plot to illustrate this (the plots are taken from one of the ensembles). More details on how the ensembles were produces can be found in section 4.4.3.

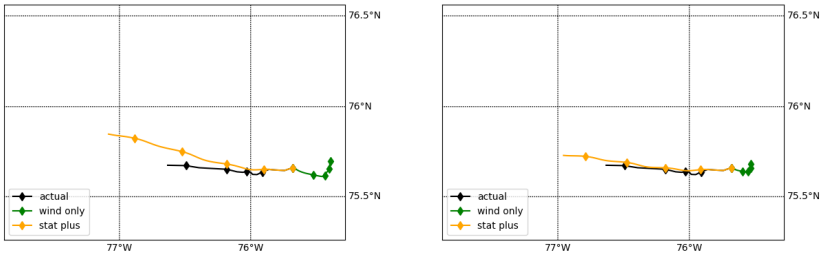

(a) Original **(b)** Wind adjusted

Figure 5.11: Plots from the statistical-plus model displayed to illustrate the effect of reducing the magnitude of the wind component. Included in each figure is the observed track, labelled *actual*, the wind component, labelled *wind only*, and the statistical-plus prediction, labelled *stat plus*. (a) show the original prediction with no adjustment of the wind track. (b) show a prediction (taken from the ensemble) where the length of the wind track has been reduced by a factor of 0.52 (the direction of the wind was also adjusted by 0.85°).

Three different ensembles were created, each using a different number of previous observations (N) to extrapolate the residual component. All sets included 100 different predictions. One set was made with N=2, one with N=6 and one with N=10. In figure 5.12 the entire ensemble of predictions with N=6 are plotted along with the observed trajectory. The predictions in this plot are distributed around the *stat plus* trajectory that is plotted in figure 5.9.

The same plot as figure 5.12, corresponding to the ensembles with N=2 and N=10, is displayed in appendix B.

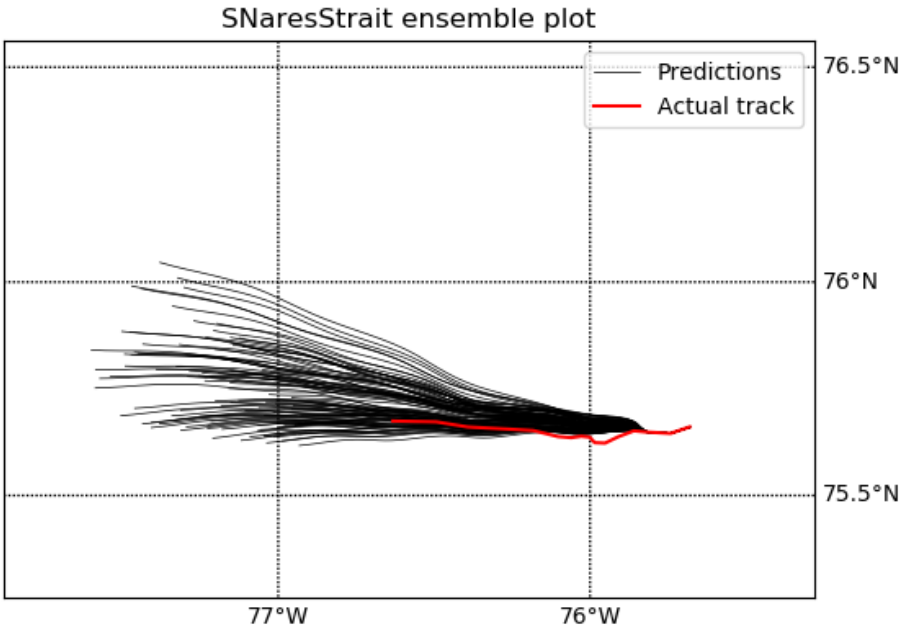

Figure 5.12: In this figure the entire ensemble of predictions (using N=6 points to extrapolate the residual) is plotted. The black trajectories are the predictions in the ensemble, while the observed trajectory is displayed in red.

Results

For each individual prediction the deviation from the observation was calculated. This data was used to estimate the variance at each point in the ensembles. In addition it was for each of the ensembles created a scatter plot like the one displayed in figure 5.13. This is a plot of the coordinates of the end points for all prediction trajectories in the ensemble for N=6 relative to the coordinates of the observed position in the same time step. This plot was created to visualizes the distribution of the ensemble relative to the actual observation.

If the prediction had been equal to the observed position, the distribution of predictions in figure 5.13 would be around the observed position. In our case, however, we see that all the predicted points are to the west/north-west of the observation. The clustering of the ensemble, in an area which does not include the observed position, suggests that there is either some systemic error in the

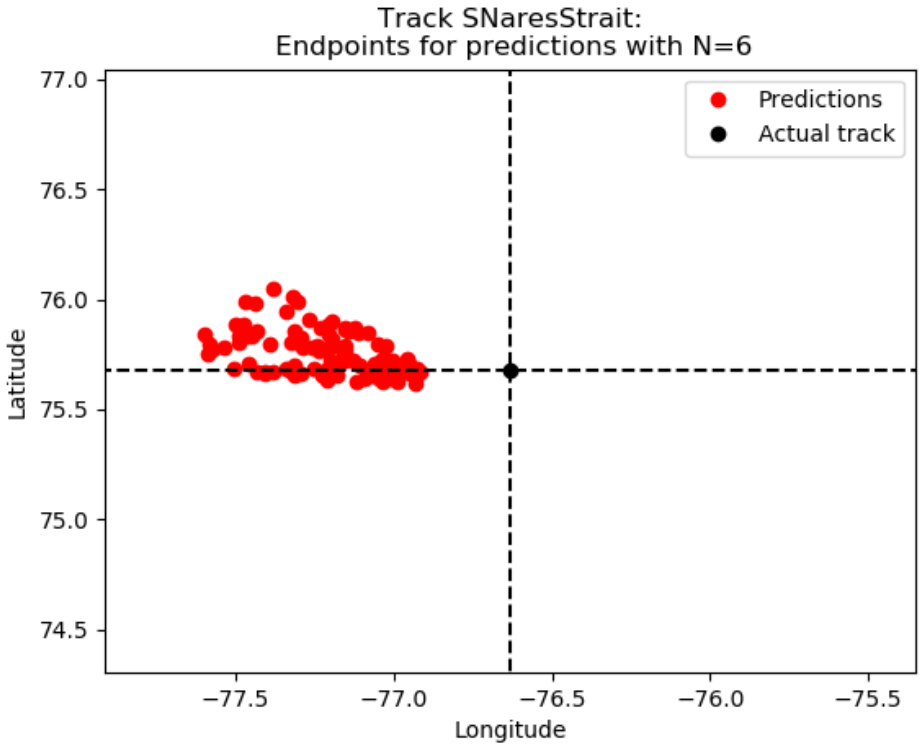

Figure 5.13: This figure display a scatter plot of the end point coordinates of the predictions, in the ensemble created with N=6, relative to the coordinates of the observed position.

model or in how the ensemble is designed. This error is not accounted for within the wind forcing uncertainty range allowed for in the ensemble. Also the other ensembles, with different N, indicates the same type of error. Plots of results from the other ensembles is displayed in appendix B.

The ensembles are used to estimate distribution parameters for the predictions. The most important among them is the SD, as this is used to determine confidence limits for the prediction. If we assume that the predictions in the ensemble are Gaussian, a model is generally not considered to be making predictions within a reasonable error range if the mean error is larger than 2SD. This distance corresponds to a confidence limit of approximately 95% for a Gaussian distribution. Ideally, most predictions should be well within this boundary if the model is to be considered operational.

The error mean and the SD for a selection time steps along the track in each of the three ensembles are listed in tables 5.2 and 5.3. From table 5.2 it is clear that the error is significantly reduced when increasing the number of points

used for extrapolate from 2 to 6. The error is further reduced by increasing the number of points from 6 to 10, but not at the same rate as from 2 to 6.

Table 5.2: This table contain the mean error at certain time steps within each ensemble. The error is measured as the deviation of the predicted trajectory from the observation. Only every 7th time step is included to represent each ensemble. Each ensemble is labelled by the number of points used to extrapolate the residual component.

Time since start	N=2	N=6	N=10
7 hours	5.637	2.795	3.144
14 hours	12.405	5.82	5.892
21 hours	19.312	8.576	7.538
28 hours	25.52	11.353	9.93
35 hours	35.775	18.267	16.093
42 hours	37.554	17.04	15.02
48 hours	41.965	18.994	16.334

Table 5.3: This table contain the standard deviation within each ensemble at certain time steps, the unit is kilometres. These values are estimated using the deviation from the observed position for each time step. Only every 7th time step is included to represent each ensemble. Each ensemble is labelled by the number of points used to extrapolate the residual component.

Time since start	N=2	N=6	N=10
7 hours	0.669	0.991	1.043
14 hours	1.341	1.361	1.232
21 hours	2.834	2.139	1.516
28 hours	4.889	3.781	3.154
35 hours	6.967	5.318	4.704
42 hours	9.395	7.466	6.877
48 hours	10.874	8.508	8.001

Figure 5.14 displays a plot including a confidence boundary around some of the points along the predicted trajectory. The radius of the boundary around each point is 2SD, for the corresponding SD at each time step. The SD-value used in the plot is the estimated value based on the ensemble analysis. This plot visualizes what the results above also indicates; there is an error in the model which is not accounted for within the wind-field variation allowed for in the ensemble.

Due to the poor results displayed in figure 5.14 the confidence boundary was increased to 3SD and a plot was created to see if this limit contained the observed position. This limit is corresponding to a confidence limit of approximately 99.7%. This limit is so close to 100% that if the observed position is not within this boundary, the prediction is almost worthless. In

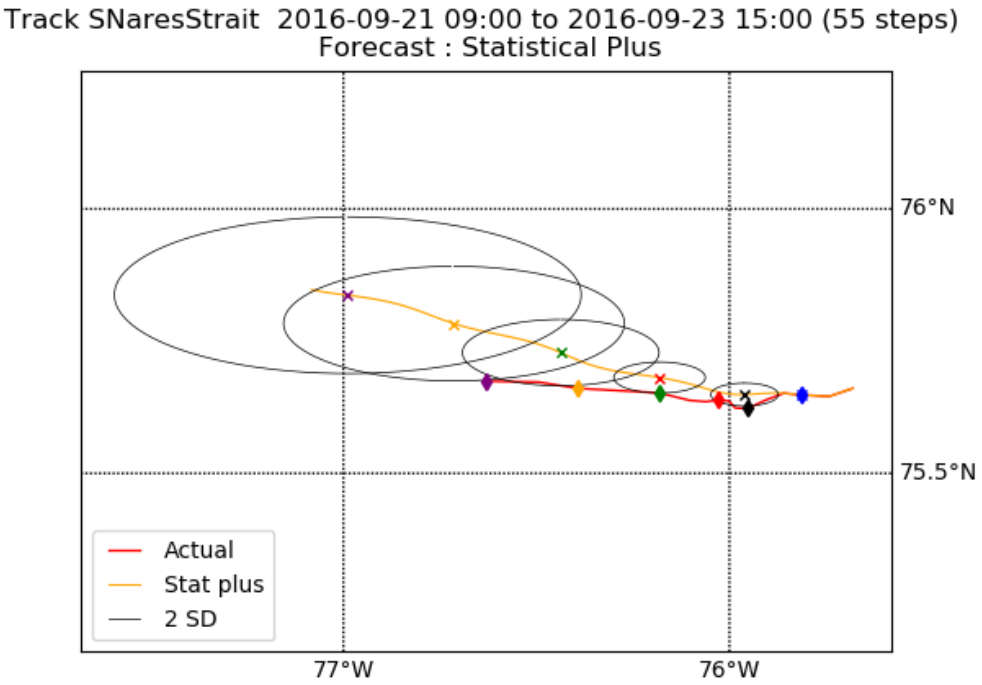

Figure 5.14: This figure display a prediction output from the statistical-plus model with N=6, labelled *Stat plus*. The observed track is included, labelled *Actual*. In addition a confidence boundary with a radius of 2SD is plotted around some of the points along the track. Each of these points is marked with a color coded ×-marker. The point on the observed trajectory for each corresponding time step is marked with a diamond marker of the same color. As is evident from the plot, the SD increases with time. The confidence boundaries are shaped like ellipses because the map projection warps the relative dimensions in x- and y-direction on the plot.

figure 5.15 both of the confidence boundaries are plotted around the endpoint in the prediction (just one point is included to make the plot easy to interpret). We can see that the prediction is within the 3SD boundary. This is a positive result and it shows that the model makes a prediction of some worth. A broader analysis of its performance could prove the prediction on this particular track section to be an outlier.

The result from the ensemble using N=10 is slightly improved compared to the one in figure 5.14. However, result from the ensemble using N=2 is much worse, and the observed prediction is not within the 3SD boundary. The result from all three ensembles indicate the same error type.

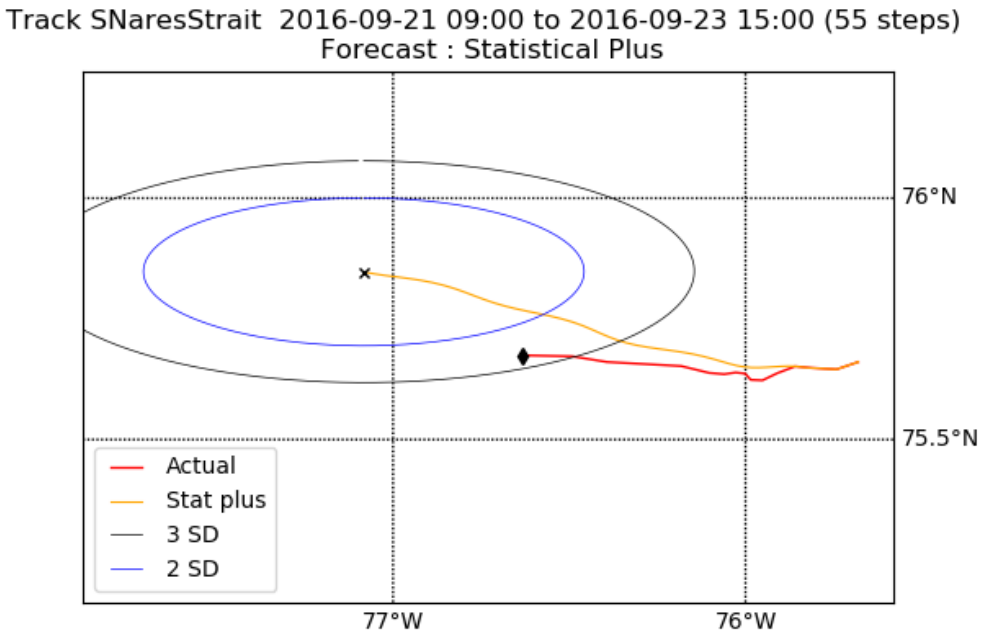

Figure 5.15: This figure display a prediction output from the statistical-plus model with N=6, labelled *Stat plus*. The observed track is included, labelled *Actual*. In addition the confidence boundaries with radius of 2SD and 3SD are plotted around the endpoint. The endpoints in the observed and predicted tracks are marked with a black ×-marker. The confidence boundaries are shaped like ellipses because the map projection warps the relative dimensions in x- and y-direction on the plot.

Figures for all ensembles are included in appendix B.

5.4.3 Discussion

It is interesting to note that the error at the end point in the original prediction trajectory was actually slightly higher than the ensemble error mean in all three ensembles. The error of the original prediction in the end points were 45.3km for N=2, 22.3km for N=6, and 19.9km for N=10. This suggests that the distribution of the predictions within each ensemble is not entirely Gaussian. It is distributed this way due to the method used to create the ensembles, particularly the number generation. The generator used produced numbers in a uniform (not a Gaussian) range.

Nevertheless, the confidence plot in figure 5.14 is considered to give a comprehensible representation of the model accuracy. We may assume that the model predictions in general are Gaussian, and interpret the results in light of this assumption. The SD from the non-Gaussian ensembles is after all just an estimation in a preliminary study.

The results from the ensemble analysis indicate a systemic error in the statistical-plus predictions. The predicted positions are more than 2SD from the observed position for most points along the track. The only points in the predicted trajectory close enough to be within the 2SD boundary are within 10 hours of the starting point. On this time scale the spatial displacement is on a relatively small scale, and correlation with the motion used to extrapolate has not yet been deprecated much. It is therefore to be expected that predictions are more accurate on this time scale.

The increased boundary displayed in 5.15 show that the prediction is within 3SD of the observation. This mean that it is not entirely improbable that the variation allowed for in the wind component accounts for the error in the prediction. If the output from this test run is an outlier. compared to an average prediction, the model may perform on a level which is suitable for operational use. However, a larger study including more test tracks must performed to draw such a conclusion.

Another notable result is that the error is halved by increasing N from 2 to 6, and further decreased increasing N to 10. This suggest that a larger interval between the points used for extrapolation is able to represent future drift more accurately. It is not possible to increase this interval indefinitely, as the forcing conditions surrounding the iceberg changes in time. It is also relative to each trajectory on what kind of time scales small changes in the direction happens, which would determine the ideal interval between the points.

It is clear for this result that the 1 hour interval (N=2) is not sufficient to represent the future drift (of this particular track). Both sets of results using longer intervals indicates that longer intervals are preferable. In many operational settings it is reasonable to expect the number of previous observations to be quite low. Therefore, it is not necessarily possible to choose the interval between the observations (like we were able to during these test runs). However, these results show the best accuracy when the interval between observations is 9 hours (N=10). Shorter intervals appears to be more vulnerable to small scale oscillations in the trajectory. The test runs did not include the use of intervals larger than 9 hours, and it can therefore not be commented on modelling using larger intervals than this.

The statistical-plus model is designed to have short term prediction capabilities.

Predictions extending longer into the future eventually loses the correlation to the initial observations. It is not reasonable to expect accurate forecasts on much longer time scales than 48 hours, which is why this was used as a limit for the test runs included in this analysis. Similar analysis could be extended to larger time scales, but the confidence boundaries on a prediction on such time scales would be huge and of limited value in any operational setting.

This ensemble analysis points to errors in either the model or the input data. For a model performing better (i.e. the observed position is well within the 2SD boundary estimated from the ensembles), we would be able to estimate the uncertainty in the model using the same kind of analysis.

This study is limited to a single track, and an extended research is necessary to draw strong conclusions about the model performance. Nevertheless, the general idea of using an ensemble for exploring forecast uncertainty is sound. To the author's knowledge, this is the first time ensembles has been used to analyse an iceberg drift model, and further research is worthwhile.

6

Conclusion

The motivation for the research presented in this thesis was the need to develop tools to accurately predict iceberg drift, due to the hazards they represent for offshore activities and shipping. A model with a known uncertainty range would be very useful for operational applications.

The dissertation started by reviewing several approaches to iceberg drift modelling. The physical principles and dynamic equations governing iceberg drift were presented, and the theory on which statistical modelling is built was discussed. Further, the computer module OpenBerg implementing two iceberg drift models were introduced. It implements one deterministic, and one statistical model utilizing dynamic components. Next, a study of the short term prediction capabilities of the two models in the computer module was performed. An attempt was made to estimate the uncertainty range of the statistical-plus model, an attempt that failed due to model errors.

Some outputs from the pure statistical model were presented in the results. This was only included to show how the statistical extrapolation is implemented, and no extensive performance analysis was included for this scheme. However, the actual accuracy of the predictions in these test runs was better than those from either of the other models.

6.1 Findings

The analysis performed in chapter 5 revealed several interesting results, summarized below:

- It was found that the dynamic iceberg drift modelling is severely limited by its dependency on input forcing data. If the forcing data is inaccurate, the predicted iceberg drift trajectory is correspondingly erroneous. The prediction output from the test runs in section 5.3 showed in particular that the input forcing field for currents, in the cases investigated in this study, was completely wrong. This agree with the statements made by Garrett (1985).

- The sensitivity study of the iceberg size parameter revealed that the size has a significant influence on the length of the predicted track. It showed that the model project larger icebergs drift slower relative to smaller icebergs. Unfortunately the poor accuracy of the prediction on the track section analysed in this thesis limited more specific analysis of the effects of changing this parameter. Also, it would be useful to have more exact measurements describing the size of the modelled iceberg. This would improve the ability to comment on how well this parameter actually describe helps guide the prediction.

- The ensemble analysis of the statistical-plus model yielded results showing large prediction uncertainty. The analysis showed that the variations allowed for in the wind trajectory did not account for this uncertainty, within the expected boundary of 2SD. This suggests that either the uncertainty source is an error in the drift model itself, or that the range of variation, allowed for in the wind data, was to small. The uncertainty was, however, accounted for within a 3SD boundary (for two of the ensembles). This means that the error in the prediction output, for the selected track, may be an extreme outlier. This call for an analysis of predictions on a larger set of tracks.

- The test runs of the pure statistical model presented in section 5.2, quite unexpectedly, provided the best results in any of the models. The statistical scheme is extremely vulnerable to changes in forcing conditions. However, these results show that under stable forcing conditions (essentially on short time intervals) the simple one term prediction scheme can be very effective.

- The good results from the statistical scheme, compared to the statistical-plus model, suggests that not only the deterministic model, but also the statistical-plus model suffers from erroneous input forcing data. The one-

term prediction, used in the statistical model, is essentially projecting a track assuming constant forcing conditions. The results show that this assumption gives a better representation of the forcing conditions than the input forcing fields (due to winds and tides) does.

- The test runs of both the statistical and the statistical-plus models gave an impression of how long the interval between observations used for the extrapolation should be. It was clear that the 1 hour interval (N=2) was not sufficient to represent the future drift. Increasing the interval yielded better results, and the recommended interval between observations (based on this study) is about 10 hours.

6.2 Future Work

The testing and study of the OpenBerg module performed in this thesis was very limited. A larger study of the performance is necessary to determine whether the results from the analysis presented in this thesis is representative of the general accuracy of the different modelling schemes.

The input data used to drive the model could also be put under closer scrutiny. It is necessary with accurate representations of the forcing conditions to be able to analyse the dynamic elements of the modelling. It was clear that the prediction error in not only the deterministic model, but also the statistical-plus model, was mainly due to error in the forcing fields. However, some last minute testing of the model was performed on tracks located at different points in time and space. These results suggest that the data give a good representation of the forcing conditions in some cases. Unfortunately it was not possible to make these test results presentable in time to include in the thesis. But they suggest that the poor prediction results presented in the thesis may have been an anomaly.

Recommended future research would include ensemble analysis of several track sections, for both the deterministic model and the statistical-plus model. It should be explored if there exist different data repositories which provide more accurate forcing data. If this is not the case, development of systems to provide improved input data are essential for both modelling schemes included in OpenBerg.

6.3 Conclusions

In chapter 1 the main objective presented was to determine whether either of the drift models implemented in the OpenBerg module are suited for operational use. The clear conclusion based on the results is not yet. Non of the models are currently suitable for operational use.

The pure statistical method appears to provide quite good accuracy, in the short term, under stable conditions. However, it is not suitable for predictions across larger time scales. The deterministic model proved to be too sensitive to inaccuracies in the input data, as has been pointed out previously (by e.g. Garrett, 1985) as a common problem in dynamic modelling. The results from the statistical model, compared to results from the statistical-plus model, show that also the statistical-plus model is sensitive to erroneous input data.

Overall, it appears that the main problem, when it comes to iceberg drift forecasting, is the accuracy of the forcing data.

Bibliography

Banke, E. and Smith, S. D. (1984). *A hindcast study of iceberg drift on the Labrador coast*. Canadian Tech Rep of Hydrography and Ocean Sci.

Barker, A., Sayed, M., Carrieres, T., et al. (2004). Determination of iceberg draft, mass and cross-sectional areas.

Batchelor, G. K. (2000). *An introduction to fluid dynamics*. Cambridge university press.

Bigg, G. R., Stevens, D. P., and Wadley, M. R. (1996). Prediction of iceberg trajectories for the north atlantic and. *GEOPHYSICAL RESEARCH LETTERS*, 23(24):3587–3590.

Bigg, G. R., Wadley, M. R., Stevens, D. P., and Johnson, J. A. (1997). Modelling the dynamics and thermodynamics of icebergs. *Cold Regions Science and Technology*, 26(2):113–135.

Carrieres, T., Sayed, M. A., Savage, S., and Crocker, G. (2001). Preliminary verification of an operational iceberg drift model. In *Proceedings of the International Conference on Port and Ocean Engineering Under Arctic Conditions*.

Dagestad, K.-F., Röhrs, J., Breivik, Ø., and Ådlandsvik, B. (2017). Opendrift v1. 0: a generic framework for trajectory modeling.

Davis, R. E. (1977). Techniques for statistical analysis and prediction of geophysical fluid systems. *Geophysical & Astrophysical Fluid Dynamics*, 8(1):245–277.

Dee, D. P., Uppala, S., Simmons, A., Berrisford, P., Poli, P., Kobayashi, S., Andrae, U., Balmaseda, M., Balsamo, G., Bauer, d. P., et al. (2011). The era-interim reanalysis: Configuration and performance of the data assimilation system. *Quarterly Journal of the royal meteorological society*, 137(656):553–597.

Dijkstra, H. A. and Ghil, M. (2005). Low-frequency variability of the large-scale ocean circulation: A dynamical systems approach. *Reviews of Geophysics*,

43(3).

Dunphy, M., Dupont, F., Hannah, C. G., and Greenberg, D. (2005). Validation of a modelling system for tides in the canadian arctic archipelago.

Dupont, F., Hannah, C., Greenberg, D., Cherniawsky, J., and Naimie, C. (2002). Modelling system for tides for the northwest atlantic coastal ocean. 221.

EI-Tahan, M., EI-Tahan, H., Venkatesh, S., et al. (1983). Forecast of iceberg ensemble drift.

El-Tahan, M. and Davis, H. (1985). Correlation between iceberg draft and above water dimensions. In *Workshop On Ice Scouring*, pages 130–147.

Garrett, C. (1984). *Statistical prediction of iceberg trajectories*, volume 7.

Garrett, C. (1985). Statistical prediction of iceberg trajectories. *Cold Regions Science and Technology*, 11(3):255–266.

Garrett, C., Middleton, J., Hazen, M., and Majaess, F. (1985a). Tidal currents and eddy statistics from iceberg trajectories off labrador. *Science*, 227:1333–1336.

Garrett, C., Middleton, J. F., Majaess, F., and Hazen, M. (1985b). *Analysis and prediction of iceberg trajectories*. Dalhousie University, Department of Oceanography.

Gaskill, H. S. and Rochester, J. (1984). A new technique for iceberg drift prediction. *Cold regions science and technology*, 8(3):223–234.

Gill, A. E. (1982). *Atmosphere—ocean dynamics*. Academic Press.

GODAE (2010). About organization. `https://www.godae-oceanview.org/about/`. Accessed: 2018-05-04.

Greisman, P., Grant, S., Blaskovich, A., and van Hardenburg, B. (1986). *Tidal propagation measurements in Baffin Bay, Lancaster Sound, and Nares Strait*. Atlantic Region Canadian Hydrographic Service Department of Fisheries and Oceans.

Hersbach, H. and Dee, D. (2016). Era5 reanalysis is in production.

Hotzel, I. S. and Miller, J. D. (1983). Icebergs: their physical dimensions and the presentation and application of measured data. *Annals of Glaciology*, 4:116–123.

Hover, F. S. and Triantafyllou, M. S. (2009). System design for uncertainty. *Mass. Inst. Technol*.

Kubat, I., Sayed, M., Savage, S. B., Carrieres, T., et al. (2005). An operational model of iceberg drift. *International Journal of Offshore and Polar Engineering*, 15(02).

Landau, L. D. and Lifshitz, E. M. (1987). *Fluid Mechanics*, volume 6. Institute of Physical Problems, U.S.S.R. Academy of Sciences, 2 edition.

Marko, J. R., Fissel, D. B., and Miller, J. D. (1988). Iceberg movement prediction off the canadian east coast. In *Natural and Man-Made Hazards*, pages 435–462. Springer.

Moore, M. (1985). Modelling iceberg motion: A multiple-time-series approach. *Canadian Journal of Statistics*, 13(2):88–94.

Murphy, D. and Anderson, I. (1985). An evaluation of the international ice patrol drift model. pages 241–255.

Pedlosky, J. (2013). *Geophysical fluid dynamics*. Springer Science & Business Media.

Press, W. H., Press, W. H., Flannery, B. P., Flannery, B. P., Teukolsky, S. A., Vetterling, W. T., and Vetterling, W. T. (1989). *Numerical recipes in Pascal: the art of scientific computing*, volume 1. Cambridge University Press.

Rick, D. (1999). Deriving the haversine formula. In *The Math Forum, April*.

Robinson, A., Carton, J., Mooers, C., Walstad, L., Carter, E., Rienecker, M., Smith, J., and Leslie, W. (1984). A real-time dynamical forecast of ocean synoptic/mesoscale eddies. *Nature*, 309(5971):781–783.

Saper, R. (2017). Openberg user's manual.

Smith, S. D. (1993). Hindcasting iceberg drift using current profiles and winds. *Cold regions science and technology*, 22(1):33–45.

Smith, S. D. and Banke, E. G. (1983). The influence of winds, currents and towing forces on the drift of icebergs. *Cold Regions Science and Technology*, 6(3):241–255.

Taylor, G. I. (1922). Diffusion by continuous movements. *Proceedings of the london mathematical society*, 2(1):196–212.

Turnbull, I. D., Fournier, N., Stolwijk, M., Fosnaes, T., and McGonigal, D. (2015). Operational iceberg drift forecasting in northwest greenland. *Cold Regions Science and Technology*, 110:1–18.

Wesche, C. and Dierking, W. (2016). Estimating iceberg paths using a wind-driven drift model. *Cold Regions Science and Technology*, 125:31–39.

A

Fundamental Fluid Dynamics

The starting premise of geophysical fluid dynamics is that the dynamics of e.g. atmospheric and oceanographic motions are determined by the systematic application of the fluid continuum equations of motions (Pedlosky, 2013).

To describe the motion, required dynamical variables are generally the density ρ, the pressure p, the velocity vector $\mathbf{u}$. In most real scenarios certain thermodynamic variables like temperature T, the internal energy per unit mass e, and the specific entropy s is also needed. Some situations may require additional variables, such as salinity, depending on the nature of the fluid. And in cases where the thermodynamic state relations are simplified, some variables may be neglected.

We will in this appendix examine which dynamical variables are relevant for iceberg drift projection, through the lens of an Eulerian kinematic description where the variables are functions of time.

A.1 Nonrotating Coordinate Frame

To begin we will state the required equations of motions in a non-rotating (inertial) frame of reference. These equations may be found in several fluid-dynamics texts (e.g Pedlosky, 2013).

The condition of mass conservation, requiring the absence of sources or sinks of mass in the fluid, is formulated by the continuity equation. The continuity equation states that the local increase of density with time must be balanced by a divergence of the mass flux $\rho\mathbf{u}$. It is expressed as

$$\frac{\partial \rho}{\partial t} + \nabla \cdot \rho\mathbf{u} = 0. \tag{A.1}$$

In equation A.1, ρ is the density, $\frac{\partial}{\partial t}$ is the time derivative, $\mathbf{u}$ is the velocity vector, and ∇ is the vectorial differential operator. Newton's law of motion for a fluid continuum can be expressed on the form

$$\rho\frac{d\mathbf{u}}{dt} = -\nabla p + \rho\nabla\phi + \mathscr{F}(\mathbf{u}). \tag{A.2}$$

Equation A.2 states that the mass per unit volume times the acceleration is equal to the sum of the pressure gradient force $-\nabla p$, the body force $\rho\nabla\phi$ (where ϕ is the potential by which the conservative body forces such as gravity can be represented) and the non-conservative forces $\mathscr{F}$. $\mathscr{F}$ may represent any non-conservative force, but in the case of ocean dynamics the main component is the frictional force within the fluid.

If the density is not considered constant, the momentum and continuity equations are insufficient to close the dynamical system. In this case one would have to consider thermodynamics to account for the variations in density. Luckily for us it is very reasonable to consider the density to be constant, as an iceberg is affected by relatively small pockets of sea water.

A.2 Rotating Coordinate Frames

The most natural frame from which to describe atmospheric and oceanic motions, is one which rotates with the planetary angular frequency Ω, due to our perspective lining on the surface of the planet. The phenomena themselves do not change with the frame of reference, but how they are described does

depend on our choice of frame. Observing an object fixed in inertial space from a rotating frame of reference, the object will appear to be rotating and accelerate (due to the curvature of its apparent trajectory).

This ambiguous viewpoint is resolved by modifying Newton's law of motion. Remember that the derived form in equation A.2 is only valid in an inertial reference frame, so we must find the altered form of the equations of motion when written entirely in terms of quantities directly observed from the rotating frame.

First consider a vector of constant magnitude $\mathbf{X}$ which rotates with the angular velocity Ω and angle α between $\mathbf{X}$ and Ω, as figure A.1 sketches.

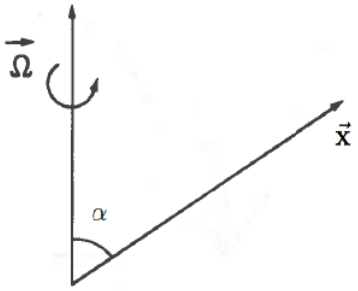

Figure A.1: $\mathbf{X}$ is a vector of constant length oriented at an angle α with respect to the axis of rotation.

For the infinitesimal time step Δt, $\mathbf{X}$ is rotated through the angle $\Delta\theta = |\Omega|\Delta t$, where $|\Omega|$ is the magnitude of Ω. Then following Pedlosky (2013), and using figure A.2 as a reference, the corresponding change in $\mathbf{X}$ is given as

$$\mathbf{X}(t + \Delta t) - \mathbf{X}(t) \equiv \Delta\mathbf{X} = \mathbf{n}|\mathbf{X}|sin\ \alpha\ \Delta\theta + O((\Delta\theta)^2), \tag{A.3}$$

where $O(\quad)$ symbolises that a variable quantity has a size exemplified by the argument, and $\mathbf{n}$ is the unit vector in the direction of change in $\mathbf{X}$. $\mathbf{n}$ must be perpendicular to both Ω and $\mathbf{X}$ due to the definition of the rotation and the fixed nature of $\mathbf{X}$. We can state this mathematically as

$$\mathbf{n} = \frac{\Omega \times \mathbf{X}}{|\Omega \times \mathbf{X}|}. \tag{A.4}$$

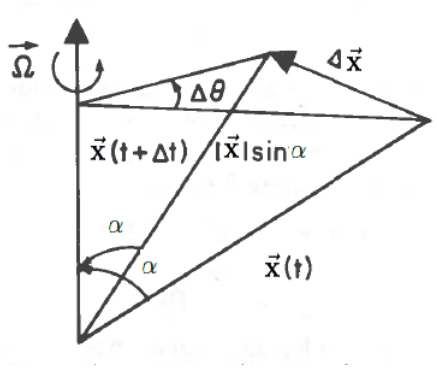

Figure A.2: **X** at a start time t and after an infinitesimal time step at time $t + \Delta t$, showing the change **X**.

In the limit where the time step goes to zero, we get

$$\lim_{\Delta t \to 0} \frac{\Delta \mathbf{X}}{\Delta t} = \frac{d\mathbf{X}}{dt} = |\mathbf{X}| sin\alpha \quad \frac{d\theta}{dt} \frac{\Omega \times \mathbf{X}}{|\Omega \times \mathbf{X}|}, \tag{A.5}$$

and as

$$|\Omega \times \mathbf{X}| = |\Omega||\mathbf{X}| sin\alpha, \tag{A.6}$$

equation A.5 for a vector **X** of fixed magnitude becomes

$$\frac{d\mathbf{X}}{dt} = \Omega \times \mathbf{X}. \tag{A.7}$$

From the perspective of an observer inside the rotating frame of reference would see no change in **X**, while an observer in a non-rotating frame would see it change as described by equation A.7. Both these observers would see the same vector, as the vector is independent of the reference frame used to describe it, but their perceptions of the rate of change of **X** will be different.

To show explicitly how the perspective is different from inside and outside the rotating frame, Pedlosky (2013) suggests that we consider an arbitrary vector **Y**. It exists in a reference frame rotating with angular velocity Ω in a Cartesian coordinate system with unit vectors along each axis $\mathbf{u}_1$, $\mathbf{u}_2$ and $\mathbf{u}_3$, as in figure A.3.

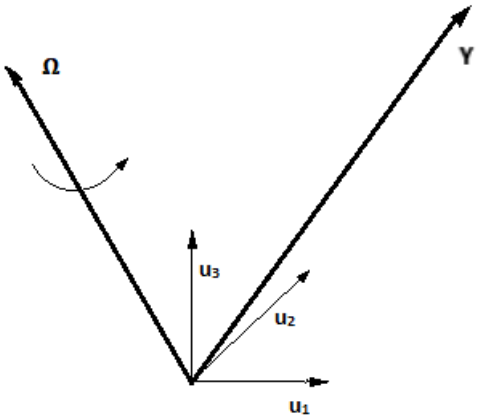

Figure A.3: Orthogonal coordinate system with base vectors $\mathbf{u}_1$, $\mathbf{u}_2$ and $\mathbf{u}_3$, and the vector $\mathbf{Y}$. The system rotates with angular velocity Ω about an axis as shown in the figure.

The vector $\mathbf{Y}$, described from the rotating reference system, can be expressed as

$$\mathbf{Y} = Y_1\mathbf{u}_1 + Y_2\mathbf{u}_2 + Y_3\mathbf{u}_3 \tag{A.8}$$

where $Y_i = \mathbf{u}_i \cdot \mathbf{Y}$ for $i = 1, 2, 3$.

The derivative in time for $\mathbf{Y}$ for an observer within the rotating frame is

$$\left(\frac{d\mathbf{Y}}{dt}\right)_R = \frac{dY_1}{dt}\mathbf{u}_1 + \frac{dY_2}{dt}\mathbf{u}_2 + \frac{dY_3}{dt}\mathbf{u}_3, \tag{A.9}$$

as the unit vectors are fixed in both length and direction. The subscript R denotes that the equation is valid inside the rotating system. For the non-rotating observer both the components of $\mathbf{Y}$ and the unit vectors change in time. Then the time derivative of $\mathbf{Y}$ for an observer outside the rotating frame will be

$$\left(\frac{d\mathbf{Y}}{dt}\right)_I = \frac{dY_1}{dt}\mathbf{u}_1 + \frac{dY_2}{dt}\mathbf{u}_2 + \frac{dY_3}{dt}\mathbf{u}_3 + Y_1\frac{d\mathbf{u}_1}{dt} + Y_2\frac{d\mathbf{u}_2}{dt} + Y_3\frac{d\mathbf{u}_3}{dt}, \tag{A.10}$$

where the subscript I denotes that the equation is valid for an observer in the non-rotating frame. Note that the scalar components Y_1, Y_2 and Y_3 are common

to both observers. Then by applying equation A.7 to each of the unit vectors we get

$$\begin{aligned} Y_1\frac{d\mathbf{u}_1}{dt} + Y_2\frac{d\mathbf{u}_2}{dt} + Y_3\frac{d\mathbf{u}_3}{dt} &= Y_1\Omega\times\mathbf{u}_1 + Y_2\Omega\times\mathbf{u}_2 + Y_3\Omega\times\mathbf{u}_3 \\ &= \Omega\times(Y_1\mathbf{u}_1 + Y_2\mathbf{u}_2 + Y_3\mathbf{u}_3) \\ &= \Omega\times\mathbf{Y}. \end{aligned} \tag{A.11}$$

Then, by inserting equation A.9 and A.11 into A.10 it yields

$$\left(\frac{d\mathbf{Y}}{dt}\right)_I = \left(\frac{d\mathbf{Y}}{dt}\right)_R + \Omega\times\mathbf{Y}. \tag{A.12}$$

In conclusion we see that the rates of change in time for the same vector **B** are perceived differently in the two frames (Pedlosky, 2013).

A.3 Equations of Motions in a Rotating Frame

If we choose a position vector of an arbitrary fluid element to be **r**, then corresponding with equation A.12 we have

$$\left(\frac{d\mathbf{r}}{dt}\right)_I = \left(\frac{d\mathbf{r}}{dt}\right)_R + \Omega\times\mathbf{r}, \tag{A.13}$$

Equation A.13 implies that the velocity observed from the non-rotating frame is equal to the velocity observed in the rotating frame in addition to the velocity due to the effects of the rotation of the body, $\Omega\times\mathbf{r}$. This may be expressed as

$$\mathbf{u}_I = \mathbf{u}_R + \Omega\times\mathbf{r}, \tag{A.14}$$

where $\mathbf{u}_I$ is the velocity seen in the non-rotaing frame and $\mathbf{u}_R$ is the relative velocity, as seen from the rotating frame. Further, Newton's laws of motion equates to the applied forces per unit mass to the acceleration in inertial space,

i.e. as the rate of change in velocity as seen in the non-rotating frame. So by applying equation A.12 to the velocity $\mathbf{u}_I$ we get

$$\left(\frac{d\mathbf{u}_I}{dt}\right)_I = \left(\frac{d\mathbf{u}_I}{dt}\right)_R + \Omega \times \mathbf{u}_I. \tag{A.15}$$

It is now necessary to eliminate $\mathbf{u}_I$ from the right hand side of equation A.15, in order to be able to describe the motions entirely in terms of quantities observed from the rotating frame of reference. To do this we apply the result from equation A.14 and get

$$\begin{aligned}\left(\frac{d\mathbf{u}_I}{dt}\right)_I &= \left(\frac{d\mathbf{u}_R}{dt}\right)_R + \frac{d\Omega}{dt} \times \mathbf{r} + \Omega \times \left(\frac{d\mathbf{r}}{dt}\right) + \Omega \times (\mathbf{u}_R + \Omega \times \mathbf{r}) \\ &= \left(\frac{d\mathbf{u}_R}{dt}\right)_R + \Omega \times (\Omega \times \mathbf{r}) + 2\Omega \times \mathbf{u}_R + \frac{d\Omega}{dt} \times \mathbf{r}.\end{aligned} \tag{A.16}$$

The difference between the perceived accelerations in the different frames is represented in equation A.16 as three additional terms. The two first terms are known as centripetal acceleration $\Omega \times (\Omega \times \mathbf{r})$, and the Coriolis force $2\Omega \times \mathbf{u}_R$, the final term $\frac{d\Omega}{dt} \times \mathbf{r}$ is the acceleration due to variations in the rotation rate.

The variation in rotation rate is negligible for oceanographic calculations, unless the time scales are large enough for the rotation rate of the Earth to change (Pedlosky, 2013). In the case of iceberg drift this variation has no significant effect on the motion and is neglected altogether, and Ω is considered a constant.

The centripetal acceleration can be expressed in terms of the perpendicular distance vector from the rotation axis to the position of the fluid element. Using this fact it allows us ultimately to express the centripetal acceleration in terms of a potential function

$$\phi_c = \frac{|\Omega \times \mathbf{r}|^2}{2} = \frac{|\Omega|^2 |\mathbf{r}_p|^2}{2}, \tag{A.17}$$

where $\mathbf{r}$ is the position vector for an element, and $\mathbf{r}_p$ is the perpendicular position vector from the rotation axis. And the expression for the centripetal

acceleration becomes

$$\Omega \times (\Omega \times \mathbf{r}) = -\nabla \phi_c. \tag{A.18}$$

This lead us to consider the centripetal acceleration as an additional force per unit mass by D'Alemberts principle (Pedlosky, 2013). And ultimately, as the centrifugal force can be expressed as this potential, it can be included in the force potential in equation A.2 to result in a total potential of

$$\Phi = \phi + \phi_c \tag{A.19}$$

This leaves us with the Coriolis acceleration which is the most interesting of the three additional terms in equation A.16, as it is the only term which explicitly involves the velocity of the fluid and is responsible for any actual structural change of the momentum equation for a uniformly rotating frame.

Note that the spatial gradients will appear identical from both the non-rotating and rotating frames. Then for an observer in a uniformly non-rotating frame, in light of the derivations above, the momentum equation A.2 becomes

$$\rho \left[\frac{d\mathbf{u}}{dt} + 2\Omega \times \mathbf{u} \right] = -\nabla p + \rho \nabla \Phi + \mathscr{F}, \tag{A.20}$$

where $\mathbf{u}$ is the velocity observed from the rotating frame. No matter from which frame of reference they are perceived, p and Φ will be the same. On the other hand the invariance of the form of the non-conservative force $\mathscr{F}$, from one reference frame to another, is relative to how it depends on the velocity field. However, for a Newtonian fluid the non-conservative forces is perceived as equal:

$$\mathscr{F}(\mathbf{u}_I) = \mathscr{F}(\mathbf{u}_R) \tag{A.21}$$

To describe the motions from the point of view of the rotating frame we move the Coriolis term to the right side of equation A.20. Note that the Coriolis force is always be perpendicular to the velocity and will not actually do any work. If we align an observer with the rotating axis, the Coriolis force appears as a force deflecting moving fluids to the right, as illustrated in figure A.4.

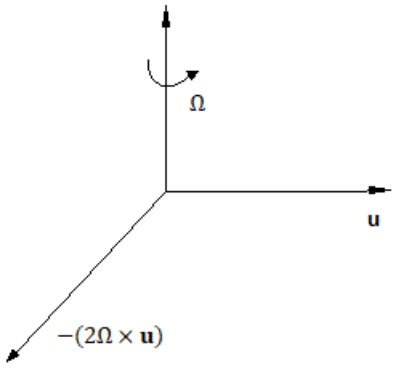

Figure A.4: The diagram represents the relation between **u**, Ω and the Coriolis force, $-2\Omega \times \mathbf{u}$ (per unit mass).

The factor 2Ω is known as the Coriolis parameter, f. It is twice the component of the angular velocity about the local vertical. This mean that for any location on the Earth's surface this parameter is given as

$$f = 2\Omega sin\varphi, \tag{A.22}$$

where Ω is the Earth's angular velocity and φ the latitude.

B

Figures

This appendix contains a list of figures displaying additional outputs from the test runs and analysis of the statistical-plus model in OpenBerg. This collection contains a selection of figures created using N=2 and N=10, corresponding figures in the main text which was all created using N=6.

These various plots visualize the significance of the time interval between the points used for extrapolation. The statistical-plus model is largely dependent the time between these extrapolation points.

B.1 Statistical-Plus Model

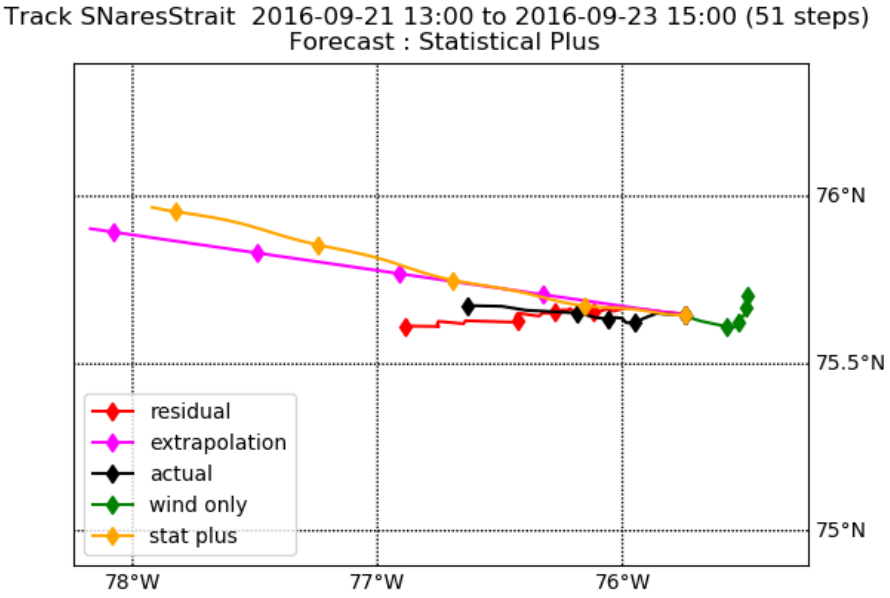

Figure B.1: Plot of observed trajectory, labelled *actual*, along with the drift forecast for the iceberg labelled SNaresStrait. This result was produced using the statistical-plus scheme, with N=2. The track labelled *wind only* is the projected component due to the wind forcing field. The track labelled *residual* is the observed track minus the wind and tidal components. The track labelled *extrapolation* is the extrapolated residual component, estimated based on the first N points in the residual track. The *stat plus* trajectory is the model prediction, it equals the sum of projected trajectories due to tides and winds as well as the extrapolated component. The tidal forcing component is not displayed in this plot, but is included in the *stat plus* trajectory.

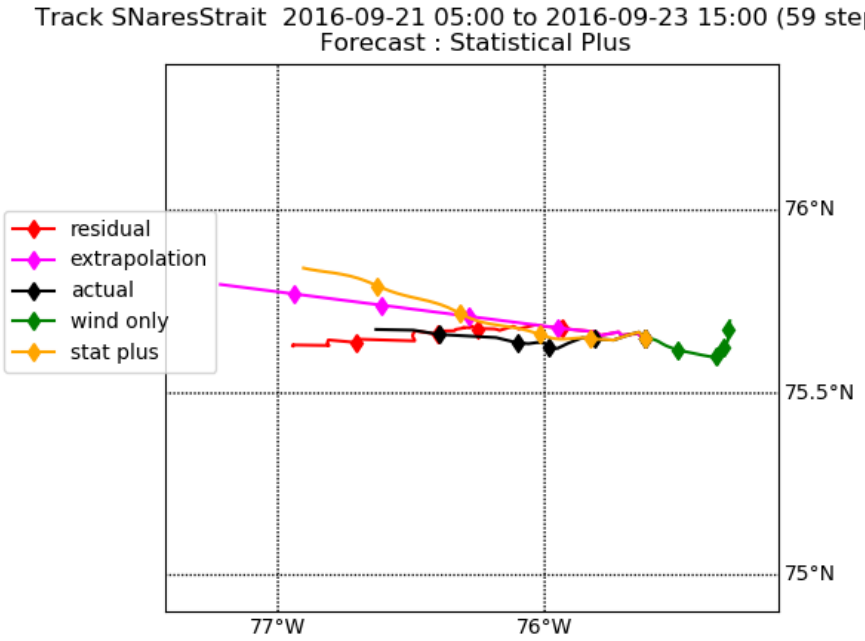

Figure B.2: Same as B.1, but for N=10.

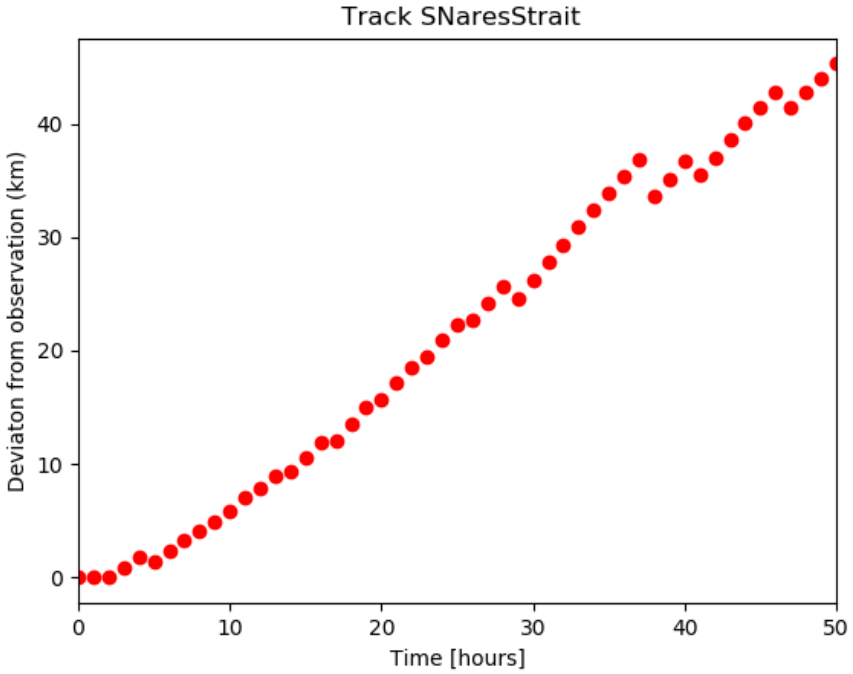

Figure B.3: Distance from the prediction to the observation, for every point along the track. This is the plot for the statistical-plus prediction with N=2, displayed in figure B.1. The x-axis is the time passed in hours, and the y-axis is the distance from the observed position to the predicted position at the corresponding time. Note that the N points used for extrapolation is included in the figure.

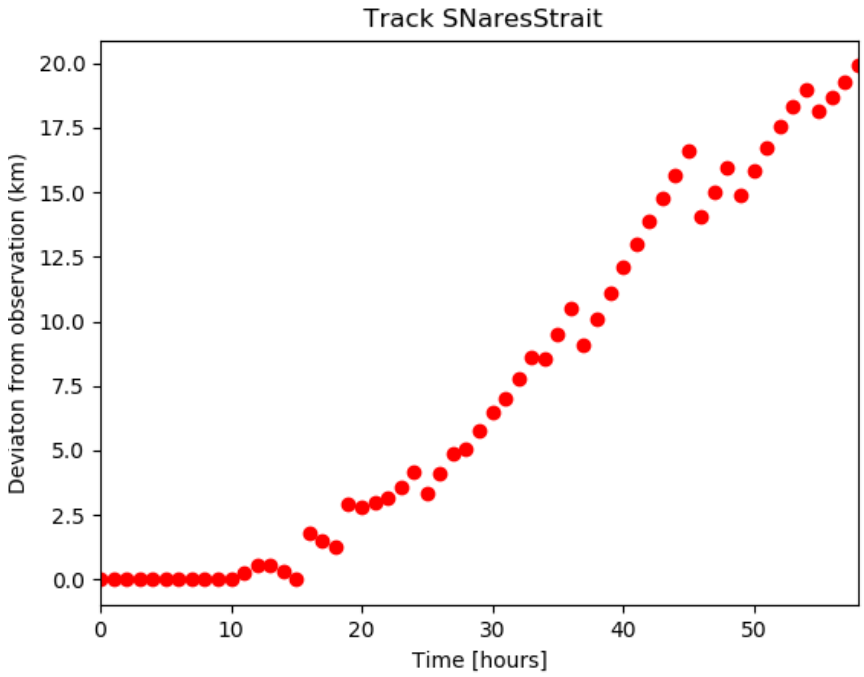

Figure B.4: Same as B.3, but for the statistical-plus prediction with N=10.

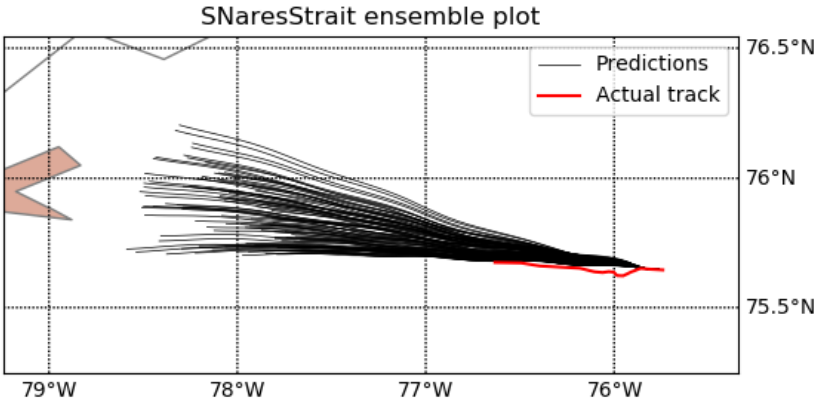

Figure B.5: In this figure the entire ensemble of predictions, using N=2 points to extrapolate the residual, is plotted. The black trajectories are the predictions in the ensemble, while the observed trajectory is displayed in red.

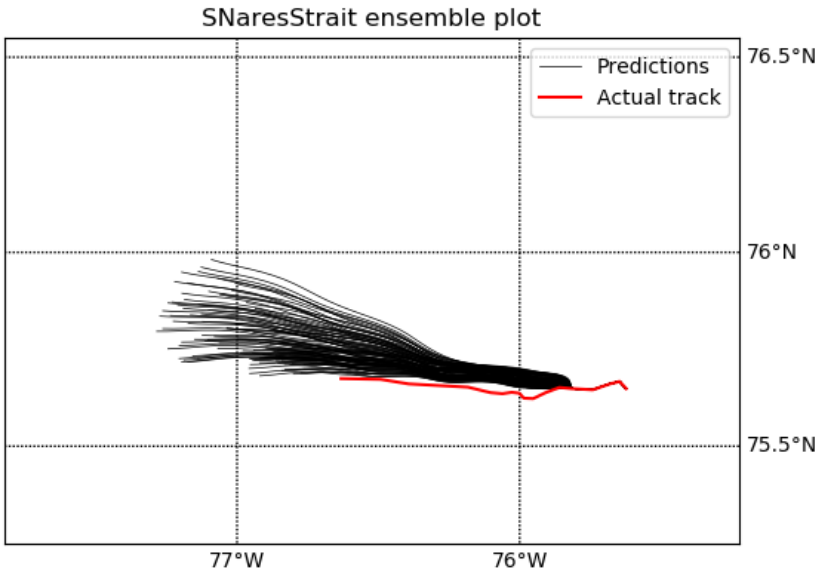

Figure B.6: Same as B.5, but for N=10.

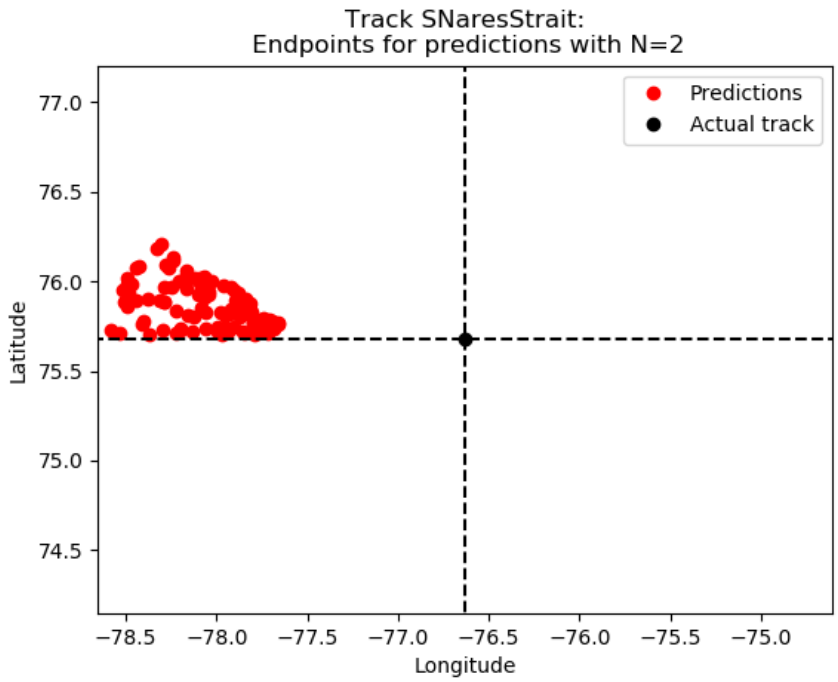

Figure B.7: This figure display a scatter plot of the end point coordinates of the predictions, in the ensemble created with N=2, relative to the coordinates of the observed position.

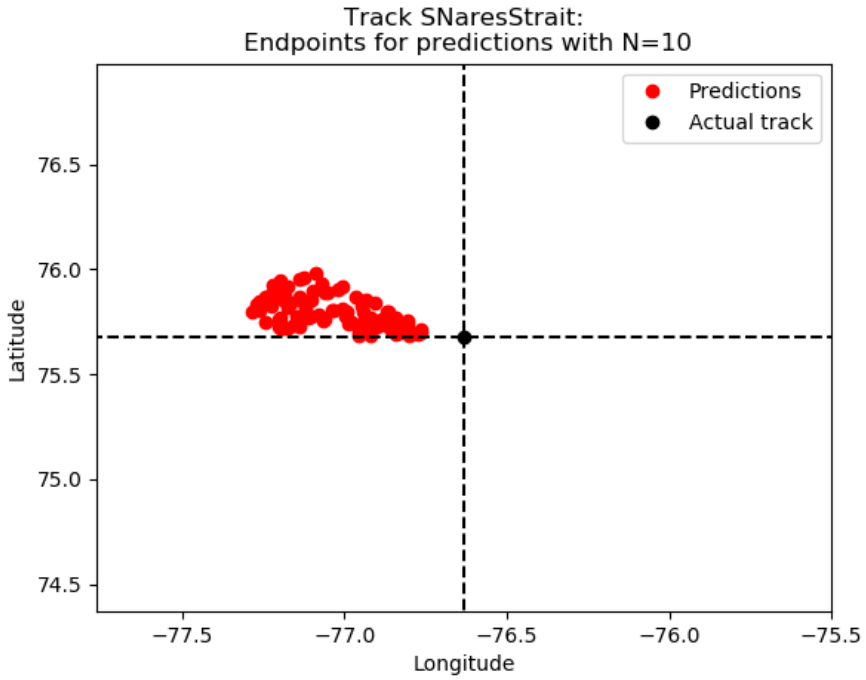

Figure B.8: Same as B.7, but for N=10.

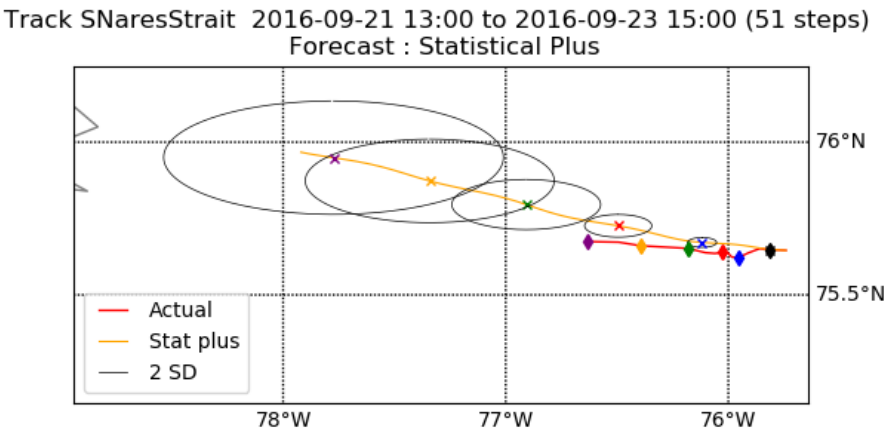

Figure B.9: This figure display a prediction output from the statistical-plus model with N=2, labelled *Stat plus*. The observed track is included, labelled *Actual*. In addition a confidence boundary with a radius of 2SD is plotted around some of the points along the track. Each of these points is marked with a color coded ×-marker. The point on the observed trajectory for each corresponding time step is marked with a diamond marker of the same color. As is evident from the plot, the SD increases with time. The confidence boundaries are shaped like ellipses because the map projection warps the relative dimensions in x- and y-direction on the plot.

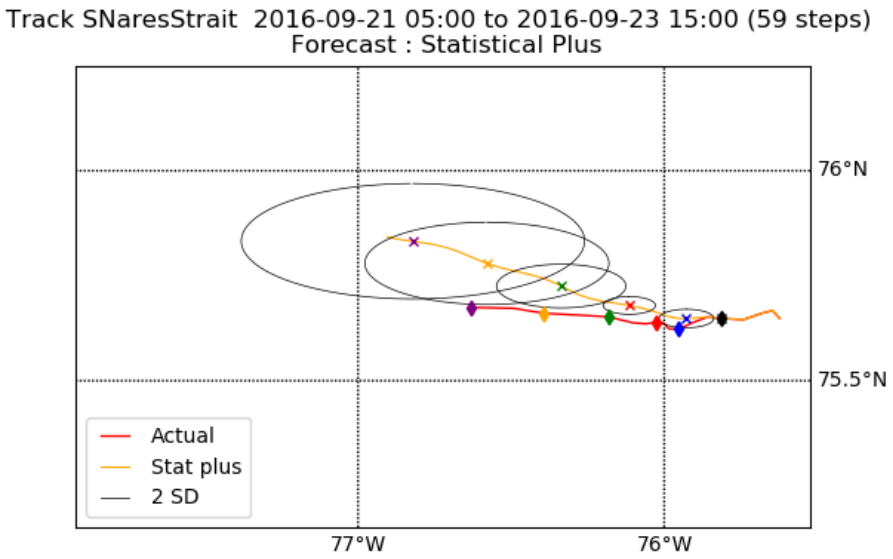

Figure B.10: Same as B.9, but for N=10.

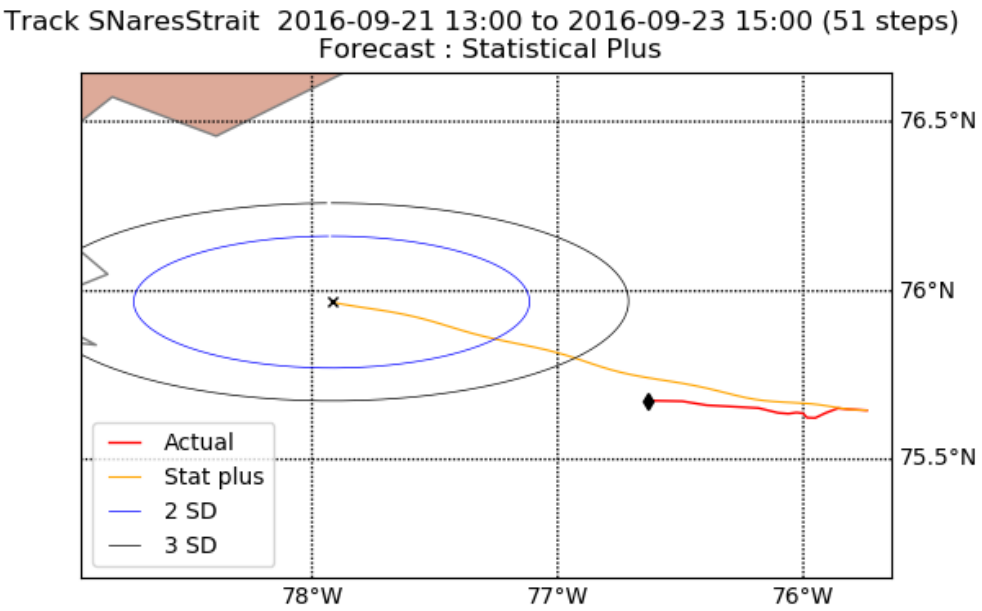

Figure B.11: This figure display a prediction output from the statistical-plus model with N=2, labelled *Stat plus*. The observed track is included, labelled *Actual*. In addition the confidence boundaries with radius of 2SD and 3SD are plotted around the endpoint. The endpoints in the observed and predicted tracks are marked with a black ×-marker. The confidence boundaries are shaped like ellipses because the map projection warps the relative dimensions in x- and y-direction on the plot.

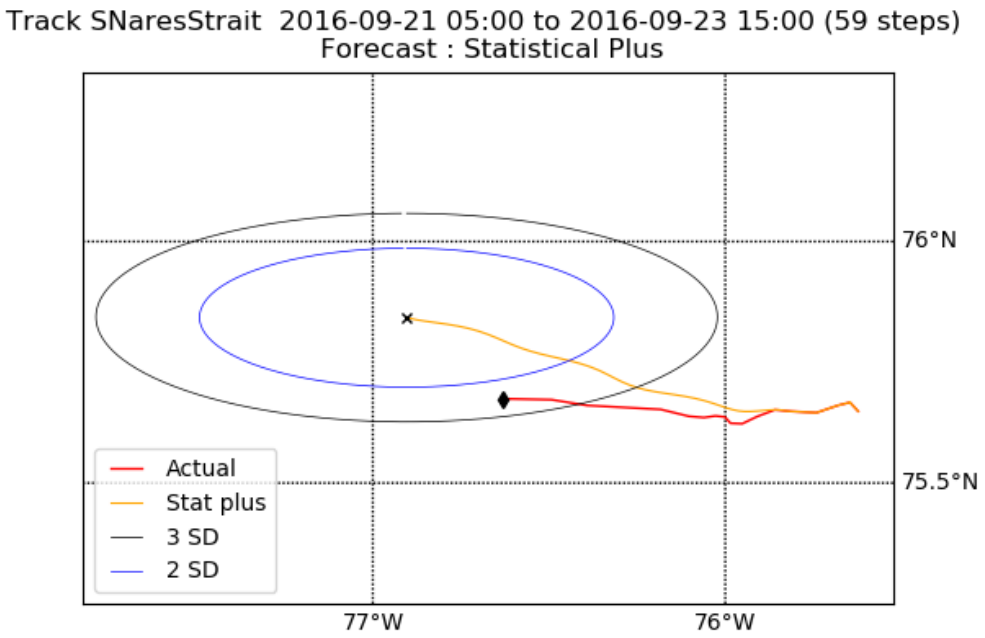

Figure B.12: Same as B.11, but for N=10.